Fall 2007

Modeling and control of freeze-form extrusion fabrication

Xiyue Zhao

Department:

MODELING AND CONTROL OF

FREEZE-FORM EXTRUSION FABRICATION

by

XIYUE ZHAO

A THESIS

Presented to the Faculty of the Graduate School of the

UNIVERSITY OF MISSOURI-ROLLA

In Partial Fulfillment of the Requirements for the Degree

MASTER OF SCIENCE IN MECHANICAL ENGINEERING

2007

_____	_____
Ming C. Leu, Advisor	Robert G. Landers, Co-Advisor

_____

Gregory E. Hilmas

PUBLICATION THESIS OPTION

This thesis consists of the following two articles that will or has been submitted for publication as follows:

1. The manuscript titled “Experimental Investigation of Effect of Environment Temperature” on Freeze-form Extrusion Fabrication” on pages 1-19 has been accepted for publication at the *Proceedings of the Solid Freeform Fabrication Symposium*, The University of Texas at Austin, Austin, TX, August 06-08 (2007).
2. The manuscript titled “Adaptive Control of Freeze-form Extrusion Fabrication Process” on pages 20-61 will be submitted to the *ASME journal of Manufacturing Science Engineering*.

ABSTRACT

Freeze-form Extrusion Fabrication (FEF) is an additive manufacturing technique that extrudes ceramic loaded aqueous pastes layer by layer below the paste freezing temperature for component fabrication. As the FEF is aimed at being conducted at low environmental temperatures, down to -20 $^{\circ}C$, it is necessary to investigate the effect of environmental temperature on the process. The advantages of fabrication at low temperature have been proved by experiments. Comparisons in terms of operation parameters, self-sustaining ability, and system dynamic response were performed at different environmental temperatures ranging from 20 $^{\circ}C$ to -20 $^{\circ}C$.

It is commonly known in paste extrusion processes that due to unmodeled effects such as air bubble release, non-uniform water content, unpredictable agglomerate breakdown, etc., the throughput (extrusion rate) is difficult to control. Moreover, during the extrusion, the rheological characteristics of the paste changes due to liquid migration, resulting in a processing challenge. Because of these difficulties, additional paste extrusion research is still in progress. Traditional PID controllers based on off-line empirical models are inadequate to control the ram extrusion processes. The Recursive Least Square algorithm is used in this research to identify the dynamic responses of the FEF process in real time. An adaptive controller with a novel general tracking control strategy is designed and implemented to regulate the extrusion force in real time. Experimental results demonstrated the robust performance of the controller, allowing the extrusion force to track various types of reference signals, while traditional controllers could only maintain the extrusion force (pressure) at a constant level (operation point).

ACKNOWLEDGMENTS

First I would like to thank my advisors, Dr. Ming Leu and Dr. Robert Landers for their great help during my Master Degree research and study. Sincere appreciation is extended to my thesis committee member Dr. Gregory E. Hilmas.

Special thanks to my colleagues Dr. Tieshu Huang and Mike Mason for their patient and warmhearted help in my research on freeze-form extrusion fabrication.

Finally, I would like to dedicate this thesis to my father Enxiang Zhao, my mother Yunxia Sun, and my friends for their love, support and encouragement.

TABLE OF CONTENTS

Page

PUBLICATION THESIS OPTION iii

ABSTRACT iv

ACKNOWLEDGMENTS v

LIST OF ILLUSTRATIONS viii

LIST OF TABLES x

NOMENCLATURE xi

INTRODUCTION 1

RERERENCES 4

PAPER

I. Experimental Investigation of Effect of Environment Temperature on Freeze-form Extrusion Fabrication 7

Abstract 7

1. Introduction 8

2. Experimental Setup and Procedure 10

2.1. Experimental setup 10

2.2. Process parameters 12

2.3. Investigation of fabrication at different temperature 12

2.3.1. Layer thickness effect 12

2.3.2. Minimum deposition angle test 13

2.3.3. Time constant and gain 13

3. Results and Discussion 14

3.1. Relationship between extrusion force and extrusion rate 14

3.2. Temperature effects 16

3.3. Comparison of part fabrication at different temperatures 17

3.3.1. Layer thickness effect 17

3.3.2. Minimum deposition angle test 18

3.3.3. Time constant and gain 20

3.4. Demonstration of components fabrication 22

4. Summary and Conclusions 23
5. Acknowledgement 24
6. References 24
II. Adaptive Control of Freeze–form Extrusion Fabrication Processes 27
Abstract 28
1.Introduction 28
2.Experimental System and Process Parameters and Disturbances 30
2.1 Hardware and Software Systems 31
2.2 Process Parameters 32
2.3 Process Disturbances 34
3.Model Parameter Variations in FEF Processes 35
3.1 Model Parameter Estimation 36
3.2 Model Variation Analysis 38
4.Adaptive Force Extrusion Controller 39
4.1 Tracking Controller Design 40
4.2 General Tracking Controller Performance 41
4.2.1 Sinusoidal Reference 41
4.2.2 Triangular Reference 42
4.2.3 Square Reference 43
4.2.4 Discussion 44
5.Summary and Conclusions 44
6.Acknowledgements 45
7.References 45
Appendix 58
VITA 59

LIST OF ILLUSTRATIONS

Figure Page

PAPER I

1. The 3D gantry system with extrusion mechanism 11
2. Schematic drawing showing the syringe and nozzle heating system. 12
3. Picture showing scrapes on a tangent ogive hollow cone. 15
4. Reference force vs. actual ram force during an extrusion process 15
5. Cylinders fabricated using the parameters in Table 1. 18
6. Definition of the minimum deposit angles 19
7. A successfully built cone (left) and a collapsed cone (right). 19
8. Minimum deposit angle as a function of temperature for different bottom diameters. 20
9. Trends of model gain and time constant at -20 °*C* and 0 °*C* 22
10. An Al2O3 and two ZrB2 tangent ogive hollow cones in the green state…… 24

PAPER II

1. Gantry motion system (left) and extrusion mechanism (right)……. 49
2. Extrusion mechanism schematic……... 50
3. FEF process control system schematic……..... 50
4. Extrusion force response to a constant command voltage of 30 mV……..... 51
5. Extrusion force (top) and command voltage (bottom).……. 51
6. Discontinuous paste flow on top of a hollow cone.. …… 52
7. Commanded voltage (upper left), modeled and measured extrusion forces (bottom left), and estimated model parameters *a* (upper right) and *b* (lower right). …..……... 52
8. Model time constant (top) and model gain (bottom) as functions of paste volume in material reservoir……..……53
9. Extrusion force (top) and command voltage (bottom) responses for a sinusoidal reference with a frequency of 0.1 *Hz*. ……..……... 53
10. Extrusion force (top) and command voltage (bottom) responses for a sinusoidal reference with a frequency of 1 *Hz*……. 54
11. Experimental extrusion force closed–loop magnitude (top) and phase shift (bottom) for sinusoidal, triangular, and square reference extrusion forces…….…….….. 54
12. Extrusion force average error (top) and error standard deviation (bottom) for sinusoidal, triangular, and square reference extrusion forces…….. 55

13. Extrusion force (top) and command voltage (bottom) responses for a triangular reference with a frequency of 0.1 *Hz*……..……... 55
14. Extrusion force (top) and command voltage (bottom) responses for a triangular reference with a frequency of 1 *Hz*…….. 56
15. Extrusion force (top) and command voltage (bottom) responses for a square reference with a frequency of 0.1 *Hz*.…… ……..…... 56
16. Extrusion force (top) and command voltage (bottom) responses for a square reference with a frequency of 1 *Hz*. ……...……...…….. 57

LIST OF TABLES

Table Page

PAPER I

1: Deposition parameters used in the layer thickness experiments..... 13

2: Results of layer thickness experiments..... 17

3: Minimum deposition test results..... 19

4: The time constant and gain of FEF at -20 °*C* and 0 °*C* 22

PAPER II

1: Estimated model time constants and gains for different batches of paste……. 48

2: Model time constants and gains for various amounts of paste in material reservoir… 49

NOMENCLATURE

Symbol	Description
a, b	model parameters
$\hat{a}, \hat{b}$	estimated model parameters
e	system error between reference and measured extrusion forces [N]
F	nominal extrusion force and [N]
F_r	reference extrusion force [N]
g	general tracking controller gain [N/mV]
K	model gain [N/mV]
u	control signal [mV]
φ	regression variable vector
η	unknown parameter vector
μ	pseudo control signal [mV]
τ	extrusion process open loop time constant [sec]
τ_d	desired closed-loop time constant [sec]

INTRODUCTION

Advanced ceramics can meet high temperature requirements and are needed for a wide range of applications in the aerospace, automotive, and other industries. Compared to conventional 3-D ceramic component fabrication techniques, which are costly and time-consuming because of mold preparation and post-sintering machining, solid freeform fabrication (SFF) has the potential of becoming an efficient and inexpensive manufacturing technique because it is a tool-less fabrication process. Recently more and more SFF techniques have been investigated and developed for ceramic processing. Well researched and commercialized SFF techniques for ceramic component fabrication include Fused Deposition of Ceramics (FDC) [1, 2], Stereolithography (SLA) [3], 3-D printing (3DP) [4, 5], and selective laser sintering (SLS) [6, 7]. Most SFF techniques for ceramic component fabrication involve the use of organic binders. In some processes, such as FDC, the binder content may reach as high as 40 to 50 vol.%. This organic binder needs to be removed during post processing and generates harmful wastes that are undesirable for the environment [8]. Freeze-form Extrusion Fabrication (FEF) uses an aqueous ceramic paste with a solids loading up to 50 vol.%. The organic binder content is only 2-4 vol. %. In FEF, aqueous-based ceramic paste is extruded using a ram extruder and deposited on a 2-D motion substrate. After the deposition of each layer, the Z-axis of the gantry system moves up by one layer thickness and the next layer is deposited. This process is repeated until the component is completely fabricated. Freeze-drying is used to prevent crack formation during the drying process. After freeze-drying, the binder is then removed in a rapid heating cycle because of the low binder content. Finally, the parts are sintered at 1550 °C for Alumina paste. FEF has some unique advantages, such as

achievability of large dimension components fabrication and a high density of sintered components. Especially, low percentage of organic binder is involved and almost no material waste is generated. Further, FEF is an environmentally friendly SFF technique.

Most research studies in extrusion processes are concerned with screw extrusion of polymer (melt) extrusion processes where most research studies have concentrated on indirect control of these variables via the regulation of melt temperature and pressure. Costin [9] gave a critical review of the early dynamics and control work in this area, which focused on classical control techniques. Hassan and Parnaby [10] used optimization and off–line curve fitting of the experimental data to define a quasi–linear steady–state model. A cascade controller with one–step–ahead forecasts of melt temperature and melt pressure calculated and changed the set points of the screw speed, barrel/die wall temperature, and restrictor valve angular position to maintain the desired extrusion rate. Costin and Taylor [11] used step tests and pseudo–random binary sequence (PRBS) tests to determine the empirical models of melt temperature and pressure in a single screw extruder (SSE). A PI controller was implemented to remove the long–term drift in the pressure level. More recently, Previdi [12] used step tests to determine an empirical first–order model from voltage (screw speed) to pressure and implemented a digital PID controller. The results showed the controller was able to regulate the pressure at a desired constant reference value. These linear techniques generally cannot capture the system's nonlinearities; therefore, they are only suitable for a specific operating point. Some nonlinear modeling techniques such as artificial neural networks, black box Nonlinear Autoregressive Network (NARX) and, more recently, grey box NARX [13] were proposed. However, these techniques are generally highly

dependent on the training data and, thus far, no controllers have been designed and implemented using these models.

Screw extrusion cannot be utilized for ceramic processing since ceramic pastes are abrasive and will severely damage the threads, eventually causing the screw extruder to fail. For ram extrusion, the pressure gradation and unstable shear stress regimes are much more complex. Modeling and controlling the extrusion pressure of the liquid–solid phase paste generally presents more difficulties, as compared to polymer extrusion, because of unpredictable disturbances such as air bubble release and agglomerate breakdown, material property uncertainties generated during the paste preparation procedures, and the complex variation of paste properties during extrusion due to liquid phase migration [14–18]. Post–operative statistical techniques such as standard error of signal, outlier, spectral and fractal analyses have been used to monitor and model the fluctuations in the ram extrusion pressure signals [19–24]. However, these approaches are still in the development stage and only a few of them have been applied to effectively provide and implement a control strategy due to the previously addressed control difficulties. Detailed initial modeling and control work for this ram extrusion process can be found in previous publication [25, 26].

RERERENCES

1. Lous, G.M., Cornejo, I.A., McNulty, T.F., Safari, A. and Danforth, S.C., 2000, "Fabrication of Piezoelectric Ceramic/Polymer Composite Transducers Using Fused Deposition of Ceramics," *J. Am. Ceram. Soc.,* **83(**1), pp. 124-28.

2. McIntosh, J.J., Danforth, S.C. and Jamalabad, V.R., 1997, "Shrinkage and Deformation in Parts Manufactured by Fused Deposition of Ceramics, "*Proceedings of the Solid Freeform Fabrication Symposium*, The University of Texas at Austin, Austin, TX, August 11-13, pp. 159-166.

3. Himmer, T., Nakagawa, T. and Noguchi, H., 1997, "Stereolithography of Ceramics," *Proceedings of the Solid Freeform Fabrication Symposium*, The University of Texas at Austin, Austin, TX, August 11-13, pp. 363-369.

4. Sachs, E.M., Cima, M.J., Bredt, J., and Curodeau, A., 1992, "CAD-Casting: The Direct Fabricaion of Ceramic Shells and Cores by Three Dimensional Printing," *Man. Rev.,* **5** (2), pp. 117-126.

5. Grau, J., Moon, J., Uhland, S., Cima, M. and Sachs, E., 1997, "High Green Density Ceramic Parts Fabricated by the Slurry-Based 3DP Process," *Proceedings of the Solid Freeform Fabrication Symposium*, The University of Texas at Austin, Austin, TX, August 11-13, pp. 371-378.

6. Kruth, J.P., Mercelis, P., Froyen, L. and Rombouts, M., 2005, "Binding Mechanisms in Selective Laser Sintering and Selective Laser Melting" *Rapid Prototyping J.*, **11**(1), pp. 26-36.

7. Subramanian, P.K., Barlow, J.W. and Marcus, H.L., 1995, "Effect of Particle Size on SLS and Post-Processing of Alumina with Polymer Binders," *Proceedings of the Solid Freeform Fabrication Symposium*, The University of Texas at Austin, Austin, TX, August 7-9, pp. 346-352.

8. Huang, T.S., Mason, M. S., Hilmas, G.E. and Leu, M.C., 2006, "Freeze-form Extrusion Fabrication of Ceramics," *Virtual and Physical Prototyping*, **1**(2), pp. 93-100.

9. Costin, M.H., Taylor, P.A., and Wright, J.D., 1982, "A Critical Review of Dynamic Modeling and Control of Plasticating Extruders," *Polymer Engineering and Science*, **22**(7), pp. 393–401.

10. Hassan, G.A. and Parnaby, J., 1981, "Model Reference Optimal Steady–State Adaptive Computer Control of Plastics Extrusion Processes," *Polymer Engineering and Science*, **21**(5), pp. 276–284.

11. Costin, M.H. and Taylor, P.A., 1982, “On the Dynamics and Control of a Plasticating Extruder,” *Polymer Engineering and Science*, **22**(17), pp. 1095–1106.

12. Previdi, F., Savaresi, S.M., and Panarotto, A., 2006, “Design of a Feedback Control System for Real–Time Control of Flow in a Single–Screw Extruder,” *Control Engineering Practice*, **14**(9), pp. 1111–1121.

13. McAfee, M. and Thompson, S., 2007, “A Novel Approach to Dynamic Modeling of Polymer Extrusion for Improved Process Control,” *Proceedings of the Institution of Mechanical Engineers, Part I: Journal of Systems and Control Engineering*, **221**(4), pp. 617–628.

14. Burbidge, A.S., Bridgewater, J., and Saracevic, Z., 1995, “Liquid Migration in Paste Extrusion,” *Chemical Engineering Research and Design*, **73**(7), pp. 810–816.

15. Amarasinghe, A.D.U.S. and Wilson, D.I., 1998, “Interpretation of Paste Extrusion Data,” *Chemical Engineering Research and Design*, **76**(A1), pp. 3–8.

16. Kaya, A. and Rice, L.S., 1982, “Measurement and Control Problems for Extrusion Processes,” *American Control Conference*, Arlington, Virginia, June, 14–16, pp. 1149–1154.

17. Amarasinghe, A.D.U.S. and Wilson, D.I., 1999, “On–Line Monitoring of Ceramic Paste Extrusion,” *Journal of the American Ceramic Society*, **82**(9), pp. 2305–2312.

18. Russell, B.D., Wilson, D.I., Lasenby, J., and Blackburn, S., 2002, “On–Line Monitoring of Pastes Undergoing Extrusion,” *Proceedings of the 4th World Congress on Particle Technology*, Sydney, Australia, July 21–25.

19. Russell, B.D., Lasenby, J., Blackburn, S., and Wilson, D.I., 2004, “Monitoring Structural Aspects of Pastes Undergoing Continuous Extrusion using Signal Processing of Pressure Data,” *Chemical Engineering Research Design*, **82**(6), pp. 770–783.

20. Russell, B.D., Ovaici, H., Lasenby, J., Beckett, S.T., and Wilson, D.I., 2006, “Real–Time Monitoring of Chocolate Extrusion by Signal Processing of Pressure Transducer Data,” *Food Control*, **17**(11), pp. 862–867.

21. Tomer, G. and Newton, J.M., 1999, “Water Movement Evaluation during Extrusion of Wet Powder Masses by Collecting Extrudate Fractions,” *International Journal of Pharmaceutics*, **182**(1), pp. 71–77.

22. Benbow, J.J., Blackburn, S., and Mills, H., 1998, “The Effects of Liquid–Phase Rheology on the Extrusion Behavior of Paste,” *Journal of Materials Science*, **33**(24), pp. 5827–5833.

23. Sherwood, J.D., 2002, “Liquid–Solid Relative Motion during Squeeze Flow of Pastes,” *Journal of Non–Newtonian Fluid Mechanics*, **104**(1), pp. 1–32.

24. Rough, S.L., Wilson, D.I., and Bridgewater, J., 2002, "A Model Describing Liquid Phase Migration within an Extruding Microcrystalline Cellulose Paste," *Chemical Engineering Research and Design*, **80**(A7), pp. 701–714.

25. Mason, M.S., Huang, T.S., Landers, R.G., Leu, M.C., and Hilmas, G.E., 2006, "Freeform Extrusion of High Solids Loading Ceramic Slurries, Part I: Extrusion Process Modeling," *Seventeenth Annual Solid Freeform Fabrication Symposium*, Austin, Texas, August 14–16.

26. Mason, M.S., Huang, T.S., Landers, R.G., Leu, M.C., and Hilmas, G.E., 2006, "Freeform Extrusion of High Solids Loading Ceramic Slurries, Part II: Extrusion Process Control," *Seventeenth Annual Solid Freeform Fabrication Symposium*, Austin, Texas, August 14–16.

PAPER I

Experimental Investigation of Effect of Environment Temperature on Freeze-form Extrusion Fabrication

Xiyue Zhao[1], Michael S. Mason[1], Tieshu Huang[1], Ming C. Leu[1], Robert G. Landers[1], Gregory E. Hilmas[2], Samuel J. Easley[3], Michael W. Hayes[3]

1870 Miner Circle

Department of Mechanical and Aerospace Engineering[1]

Department of Materials Science and Engineering[2]

University of Missouri-Rolla, Missouri, U.S.A. 65401

The Boeing Company, St. Louis, Missouri 63042[3]

{xzd2c, mmason, hts, mleu, landersr, ghilmas}@umr.edu

{Michael.w.hayes2, samuel.j.easle}@boeing.com

Abstract

Freeze-form Extrusion Fabrication (FEF) is an additive manufacturing technique that extrudes ceramic loaded aqueous pastes layer by layer below the paste freezing temperature for component fabrication. A computer controlled 3-D gantry system has been developed for the FEF process. The system includes a temperature control subsystem that allows for fabrication of components below the paste freezing temperature. The low temperature environment allows for larger component fabrication. Comparisons in terms of layer thickness, self-sustaining ability, and system response were performed between 0 °C and -20 °C for alumina sample fabrication. The minimum deposition angles without use of support material have been determined for 20°C, 10 °C, 0 °C, -10 °C and -20 °C fabrication.

Keywords: Ram extrusion, Ceramic, Alumina, Temperature effect, RLS, Rapid Prototyping

1. Introduction

Advanced ceramics which can meet high temperature requirements are needed for a wide range of applications in the aerospace, automotive, and other industries. Compared to conventional 3-D ceramic component fabrication techniques, which are costly and time-consuming because of mold preparation and post-sintering machining, solid freeform fabrication (SFF) has the potential of becoming an efficient and inexpensive manufacturing technique because it is a tool-less fabrication process [1]. Recently more and more SFF techniques have been investigated and developed for ceramic processing. Well researched and commercialized SFF techniques for ceramic component fabrication include Fused Deposition of Ceramics (FDC) [2, 3], Stereolithography (SLA) [4], 3-D printing (3DP) [5, 6], and selective laser sintering (SLS) [7, 8]. In the FDC process, the ceramic-thermoplastic material is heated into a semi-liquid state and extruded through a nozzle. The extruded material is deposited on an X-Y working surface in a layer by layer fashion. The solids loading is typically 40-50 vol.%. FDC uses a high percentage of organic chemical binders at 40-50 vol.% [3]. Stereolithography of ceramic components is implemented by mixing resins with ceramic particles which can be polymerized when exposed to ultraviolet light. However, the laser scattering at the ceramic particles reduces the cure depth and widens the cured area, thus reducing the dimension accuracy [4]. 3-D printing of ceramic components includes two approaches according to applied materials: hot-melt dry powder and aqueous based pastes. The dry powder method is similar to 3-D printing where the binder is selectively printed onto the powder bed [5]. The main concern of this method is the relatively low green density, only up to 35 vol. %. In recent years aqueous based ceramic pastes were

explored to overcome this problem [6]. Selective laser sintering was applied in ceramic part fabrication by mixing organic binder (typically PMMA) with ceramic particles as the process material allowing for achieving a smooth surface finish [7], but the post-sintering density is relatively low at about 55 vol.% [8].

Most SFF techniques for ceramic component fabrication involve the use of organic binders. In some processes, such as FDC, the binder content may reach as high as 40 to 50 vol.%. This organic binder needs to be removed during post processing and generates harmful wastes that are undesirable for the environment [9]. Freeze-form Extrusion Fabrication (FEF) extended the idea of the rapid freeze prototyping (RFP) method [10-13], where water droplets are deposited on demand and freeze on a 2-D motion substrate for the fabrication of 3D components in a layer-by-layer manner. FEF uses an aqueous ceramic paste with a solids loading up to 50 vol.%. The organic binder content is only 2-4 vol. %. In FEF, aqueous-based ceramic paste is extruded using a ram extruder and deposited on a 2-D motion substrate. After the deposition of each layer, the Z-axis of the gantry system moves up by one layer thickness and the next layer is deposited. This process is repeated until the component is completely fabricated. Freeze-drying is used to prevent crack formation during the drying process. After freeze-drying, the binder is then removed in a rapid heating cycle because of the low binder content. Finally, the parts are sintered at 1550 °C for Alumina paste. Post-FEF processing has been detailed in previous publications [1, 9]. FEF has some unique advantages, such as achievability of large dimension components fabrication and a high density of sintered components. Especially, low percentage of organic binder is involved and almost no material waste is generated. Further, FEF is an environmentally friendly SFF technique.

In this paper, a custom-designed 3D gantry system and a custom-designed cooling system (0 °C to -30 °C) was used for FEF processing. The layer thickness optimization was performed for fabrication at -20 °C. The self-sustaining ability at different temperatures was analyzed. The time constant and gain of the first-order process model of FEF were calculated. The trends of these two parameters during fabrication at -20 °C and at 0 °C were recorded and analyzed.

2. Experimental Setup and Procedure

2.1. Experimental setup

The 3-D gantry system, as shown in Figure 1, consists of three orthogonal linear axes from Velmex BiSlide (Velmex, Bloomfield, NY), each with a 508 *mm* travel range. The X-axis consists of two parallel slides and is used as the support for the Y-axis. The two parallel slides provide smooth and stable motion and allow more fabrication space. The Z-axis is mounted on the Y-axis and the extrusion mechanism is mounted on the Z-axis. All these axes are mounted with limit switches on both ends. Four DC motors (Pacific Scientific PMA22B), each with a resolver for position feedback at a resolution of 1000 counts per revolution, drive the axes. Each motion axis has a maximum speed of 127 *mm/s* and a resolution of 0.00254 *mm.* All the axes are controlled by a Delta-Tau Turbo PMAC PCI board.

The right image in Figure 1 shows an enlarged view of the extrusion mechanism. It is a ram extruder driven by a DC motor (Kollmorgen AKM23D), which has an encoder with a resolution of 0.254 μm and is mounted on the Z-axis slide. A load cell (Omega LC305) is mounted between the plunger and the ram extruder to measure the extrusion

force. An analog-to-digital conversion board (Delta-Tau ACC28) converts the analog signal from the load cell to a digital signal and is input to the PMAC board.

The 3-D gantry is located inside a freezer. A condenser is used to keep the freezer temperature at 0 °C (± 2 °C). Liquid nitrogen is used for lowering the temperature to the range of 0 °C to –30 °C. A temperature controller (Omega CN132) (Danaher Motion, Wood Dale, IL) is used to control the temperature of the freezer by turning a solenoid valve on or off, which regulates the flow rate of nitrogen. As shown in Figure 2, two heating coils are installed around the extruder and the nozzle to keep the paste temperature in the range of 10~15 °C to prevent the paste from freezing.

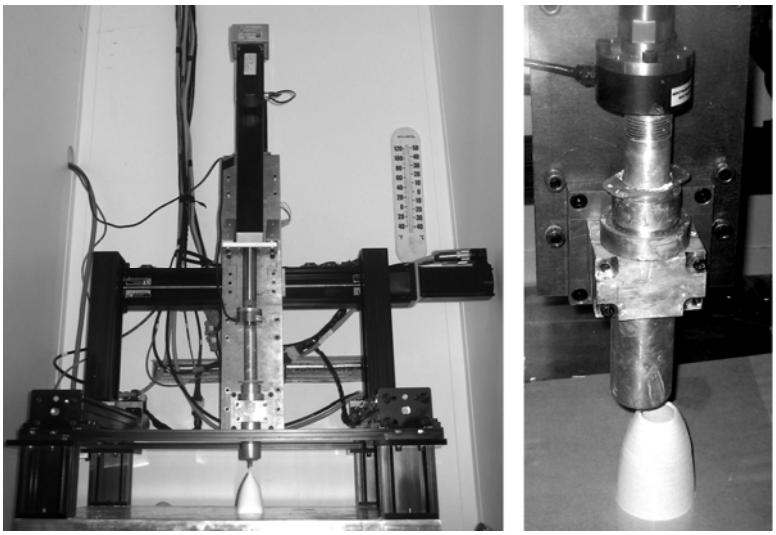

Figure 1: The 3D gantry system with extrusion mechanism.

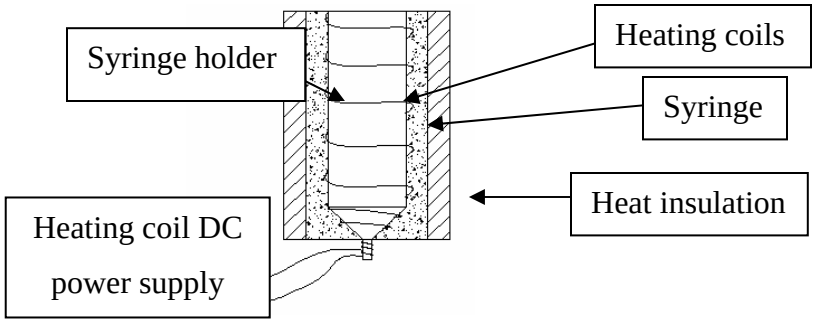

Figure 2: Schematic drawing showing the syringe and nozzle heating system.

2.2. Process parameters

The process parameters included initial extrusion force, extrusion force increment, road offset, layer thickness, and X-Y motion table (working surface) speed. The road offset between deposition trajectories was mainly determined by the diameter of the nozzle. 580 μm diameter nozzles were used in all experiments. The X-Y table speed is 10 *mm/s*.

The extrusion force is directly related to extrusion rate. A larger extrusion force is associated with a higher extrusion rate, and vice versa. The initial extrusion force was set to 311 *N*. To maintain a constant extrusion rate and avoid nozzle clogging, the reference extrusion force was continually increased at 2.2×10^{-2} *N/s*. An adaptive PI controller was designed and implemented to control the ram velocity in a range of ± 50 $\mu m/s$ at steady state to achieve the desired extrusion.

2.3. Investigation of fabrication at different temperatures

2.3.1. Layer thickness effect

The layer thickness determined by the Z-axis shift distance needs to be carefully adjusted, in order that the nozzle does not disturb the previous layer during the deposition process. To optimize this parameter, cylinder samples were fabricated at 0 °*C* and -20 °*C* with different layer thicknesses and X-Y table speeds, as listed in Table 1. The table

speed for fabrication at -20 °*C* (11 *mm*/*s*) was slightly larger than at 0 °*C* (10 *mm*/*s*) to compensate for the temperature effect of the paste.

Table 1: Deposition parameters used in the layer thickness experiments

	Temperature (°*C*)	**X-Y table speed (*mm/s*)**	**Layer thickness (*μm*)**
1	0	10	510
2	-20	11	510
3	-20	11	580
4	-20	11	640

2.3.2. Minimum deposition angle test

The minimum deposition angle is the minimum angle that can be achieved between the substrate and the slope of a hollow cone without collapse. This angle reflects the offset ability of the FEF process in building a 3-D part without supporting material. Three set of tests were conducted to fabricate cones with different bottom diameters to find the minimum deposit angle. The tested temperatures include 20 °*C*, 10 °*C*, 0 °*C*, -10 °*C,* and -20 °*C*. In each set of tests, hollow cones were fabricated using bottom diameters of 38 *mm*, 51 *mm,* and 64 *mm*. The cone height was varied to determine the lowest height without collapse for minimum deposition angle calculation.

2.3.3. Time constant and gain

The FEF process contains many nonlinear effects, such as air bubbles trapped within the paste, uneven water content from the upper portion to the bottom portion of the paste, various sizes of agglomerates, etc. Paste consistency is also slightly different from batch to batch. These factors contribute to difficulties in modeling the extrusion process.

Previous research work shows that the extrusion process, in general, can be approximated as a first-order dynamic system, where commanded voltage to the ram motor amplifier is the input and extrusion force is the output [10]. However, according to the experimental data, there is significant variation in the model parameters. Therefore, the Recursive Least Square (RLS) method will be applied to model the extrusion process and determine how the amount of remaining paste in the material reservoir affects the dynamic model parameters. The model input is the commanded ram motor voltage, which is processed by a 16 bit digital-to-analog converter before going to the ram motor amplifier. The output is the measured extrusion force, which is sent to the computer via an analog-to-digital converter. The resolution of the measured extrusion force is 2.2 *N*.

Experiments were conducted to investigate how the parameters of the extrusion force dynamic model varied. In these experiments, a command ram motor voltage of 3 mV is sent to the motor amplifier for 10 seconds, and then the voltage is changed to -1.5 mV for 5 seconds, increased to 3.75 mV for another 10 seconds, and decreased to -1.75 mV for 5 seconds. Each test lasted until approximately 5 *ml* of paste was extruded. The extrusion force was measured with a sample period of 0.06 *sec* and the RLS method was applied to estimate the model parameters at each sample period. The experiments were repeated at two environmental temperatures.

3. Results and Discussion

3.1. Relationship between extrusion force and extrusion rate

During fabrication the extrusion rate decreased as the amount of paste in the syringe decreased when the extrusion force was constant. The table speed was maintained constant during fabrication. Therefore, the decrease of extrusion rate may result in under-

filling and generating scraps in the building area as shown in Figure 3. The reason for this phenomenon is still not clear, but may be related to a change of the rheology of the paste during extrusion. In effect, there may be a redistribution of liquid phase versus solid phase during the extrusion process.

The extrusion force should be gradually increased to balance the gradual increase of the resistance force of paste during extrusion which may be caused by this liquid migration. By using the adaptive PI controller at a sample period of 0.06 seconds, the extrusion force followed the increasing reference force closely as shown in Figure 4.

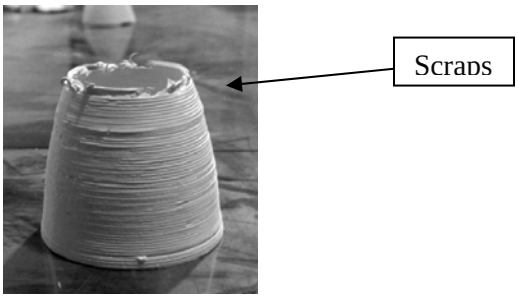

Figure 3: Picture showing scrapes on a tangent ogive hollow cone.

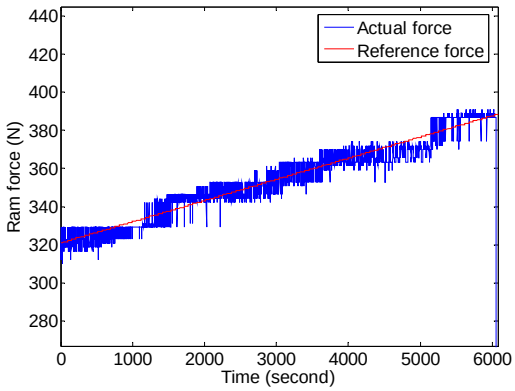

Figure 4: Reference force vs. actual ram force during an extrusion process

3.2. Temperature effects

At 20 °C, the drying rate of the extruded materials was found to be significantly high when processed out of the freezer where the moisture was less than 60%. The high drying rate was usually associated with non-uniform drying, which generated cracks and caused warping. Increasing moisture in the surrounding area could help in improving sample quality.

At 0 °C and processed in the freezer, water evaporated more slowly and the drying rate is observed lower than that at 20 °*C*. The surface finish of the samples fabricated at this temperature was generally smoother than the surface finish of those fabricated at 20 °*C*.

Because the extruded materials didn't freeze, the lower portion of the component did not have enough strength to support the whole component toward the end of the fabrication cycle during large component fabrication. This led to component deformation or even collapse. Decreasing the table speed (< 12.5 *mm/s*) could help solve this problem. However, the slow deposition rate would increase the fabrication time, which is undesirable.

At -20 °C, heating coils (Figure 2) were needed to keep the paste warm (10-15 °*C*) to ensure proper extrusion. The extruded ceramic paste could freeze at -20 °*C*. No visible part deformation was observed. The table speed used for fabrication at -20 °*C* was 15-20 *mm/s*, while 10-12 *mm/s* were used for fabrication at 0 °*C*. Table 2 shows the general comparison of fabrication at these three temperatures.

Table 2: Results of layer thickness experiments

Environment Temperature (^{o}C)	Drying Rate	Freezing Rate	Table Speed (mm/s)	Part Deformation	Part Surface Condition
-20	Low	High	15-20	No	Smooth
0	Medium	None	10-12	Yes	Smooth
20	High, non-uniform	None	10-12	Yes	Cracks and warping

3.3. Comparison of part fabrication at different temperatures

3.3.1. Layer thickness effect

Five cylinders were fabricated for each layer thickness. Figure 5 shows one typical cylinder for each value listed in Table 1. Cylinder 1 was fabricated at 0 °*C*, while cylinders 2-4 were fabricated at -20 °*C*. Visually cylinder 1 has the best surface finish. This is because at this temperature, the extruded paste had a high viscosity (>50 *Pa-s*). As a result, the new layer of material deformed slightly, making the surface smoother. The layer thickness for this fabrication was 510 μm, which was slightly less than the diameter of the nozzle (580 μ*m*). At –20 °*C*, the paste froze quickly and exhibited little deformation. When using the same layer thickness (510 μm), the surface quality was poor as shown in Figure 5 (cylinder 2). This is because the paste did not deform and the nozzle tip would scratch the previously deposited material. By increasing the layer thickness to 580 μm, the cylinder (Figure 5, cylinder 3) had a better surface finish. When the layer thickness was increased to *640* μm, the cylinder (Figure 5, cylinder 4) had an even better surface finish. However, if the layer thickness were larger than 640 μm, under-filling

would occur. Therefore, the optimized layer thickness should be close to 640 μm for fabrication at -20 °C.

Experiments were repeated at table speeds of 15 *mm/s* and 20 *mm/s* and results indicated no direct relationship between table speed and layer thickness distance.

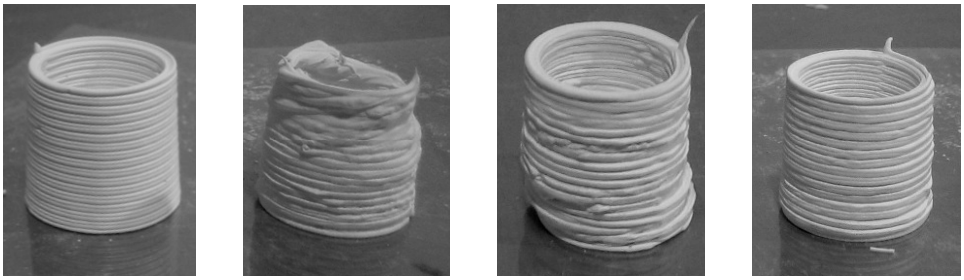

1 (0°C, 510 μm) 2 (-20°C, 510 μm) 3 (-20°C, 580 μm) 4 (-20°C, *640* μm)

Figure 5: Cylinders fabricated using the parameters in Table 1.

3.3.2. Minimum deposition angle test

The minimum deposition angle test results are shown in Table 3. Figure 6 gives the definition of the minimum deposition angle. Figure 7 shows a successfully built cone having a 19 *mm* height and a 38 *mm* bottom diameter (left) and a collapsed cone (right).

Figure 8 shows the relationship between the minimum deposit angle and the fabrication temperature. The minimum deposition angles increased quickly from -20 °C to 0 °C, then more slowly from 0 °C to 10 °C, and the trend flattened from 10 °C to 20 °C. At -20 °C, the extruded materials froze and became solid immediately, thus providing the lowest minimum deposition angle. When the temperature increased to 0 °C, the extruded materials would not freeze, but the viscosity was high. As the temperature increased, the viscosity became lower and the minimum deposition angle increased.

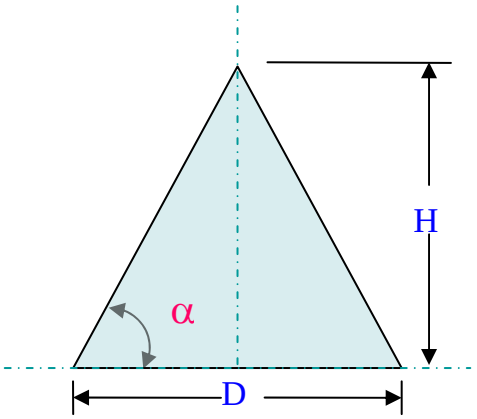

Figure 6: Definition of the minimum deposit angles.

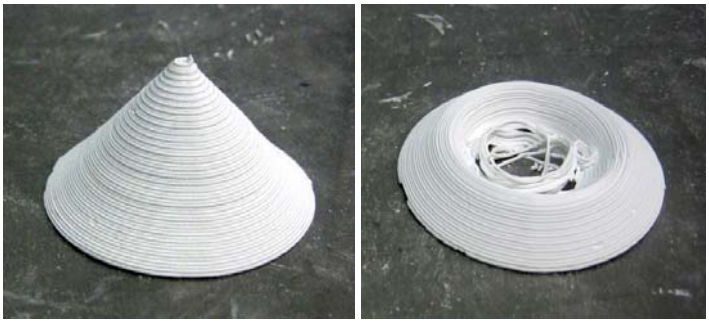

Figure 7: A successfully built cone (left) and a collapsed cone (right).

Table 3: Minimum deposition test results

Fabrication Temperature (°C)	**Bottom Diameter = 38 (*mm*)**	**Bottom Diameter = 51 (*mm*)**	**Bottom Diameter = 64 (*mm*)**
	Collapse angle (°)	**Collapse angle (°)**	**Collapse angle (°)**
-20	27.47	25.64	23.75
-10	34.22	34.61	34.53
0	37.72	41.35	43.35
10	38.66	45.58	49.04
20	40.91	47.73	50.57

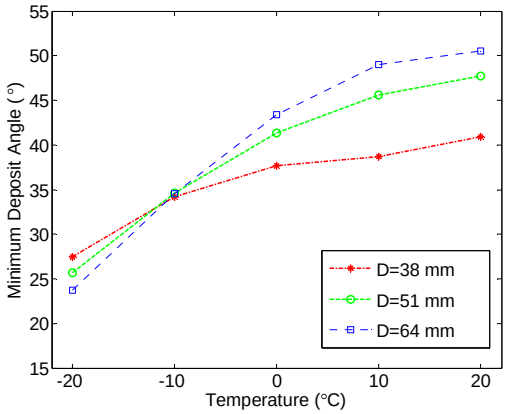

Figure 8: Minimum deposit angle as a function of temperature for different bottom diameters.

3.3.3. Time constant and gain

It has been shown that the dynamics of the extrusion force process can be modeled by a first order process [10]. In this section, the effect of environment temperature on the model parameters was explored. The transfer function of the first-order process in the digital domain is

$$G(z) = \frac{F(z)}{V(z)} = \frac{K(1-a)}{z-a} \tag{1}$$

where z is the forward shift operator, F is the ram force (N), and V is the DC voltage sent to the ram motor amplifier. The difference equation corresponding to equation (1) is

$$F(k) = aF(k-1) + K[1-a]V(k-1) = \boldsymbol{\eta}\boldsymbol{\varphi} \tag{2}$$

where k is the iteration number and the unknown parameter and regression variable vectors, respectively, are

$$\boldsymbol{\eta} = \begin{bmatrix} a & K(1-a) \end{bmatrix} = \begin{bmatrix} a & b \end{bmatrix} \tag{3}$$

$$\boldsymbol{\varphi} = \begin{bmatrix} F(k-1) & V(k-1) \end{bmatrix}^T \tag{4}$$

In this form, the Recursive Least Squares technique can be applied to the experimental data to estimate the parameters a and b. The model parameters (i.e., time constant τ and gain K) are derived from the estimated parameters a and b and, respectively, are

$$\tau = -\frac{T}{\ln a} \tag{5}$$

$$K = \frac{b}{1-a} \tag{6}$$

Table 4 shows the model time constants and gains for six experiments at 0°C and six experiments at -20°C. The model time constants and gains for each experiment were calculated by taking the average of the last 100 data points of the total data gathered in each experiment. The data is graphed in Figure 9. The model time constant and gain for the model at -20°C showed the same trend as those at 0°C: the time constant decreased and gain increased as the initial volume of paste in the material reservoir decreased. As paste is extruded, air bubbles leave and liquid migration occurs causing the paste to become drier and stiffer. These effects cause the time constant to decrease and the gain to increase. The model time constant in each experiment at -20°C was smaller than the corresponding time constant at 0°C and the model gain at -20°C was also lower than the corresponding model gain at 0°C. The reason for this is that the paste temperature at -20 °C was increased 10~15°C by the heater; therefore, the paste temperature was higher than the paste in the 0°C experiments, making the paste thinner and easier to extrude.

Table 4: The time constant and gain of FEF at -20 °*C* and 0 °*C*

Test	Volume of remaining paste (*ml*)	FEF at -20 °*C*		FEF at 0 °*C*	
		Time constant (*s*)	Gain (*N/mV*)	Time constant (*s*)	Gain (*N/mV*)
1	35	108.03	761.38	117.79	794.66
2	30	95.58	825.51	110.36	881.46
3	25	85.47	889.93	103.52	920.43
4	20	75.72	931.06	91.27	935.82
5	15	65.28	936.75	87.69	980.16
6	10	40.32	973.61	61.43	1035.18

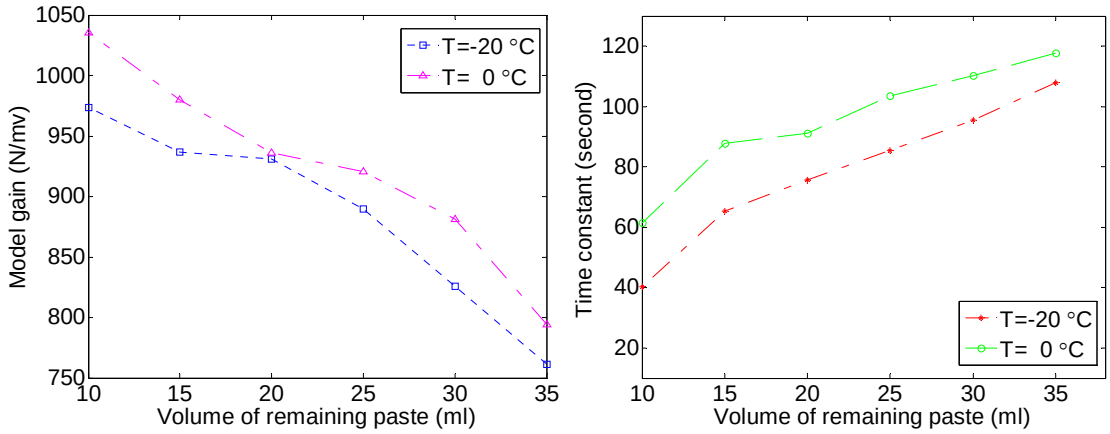

Figure 9: Trends of model gain and time constant at -20 °*C* and 0 °*C*.

3.4. Demonstration of components fabrication

Figure 10 shows tangent ogive cones in the green state fabricated at -20 °*C*. The left image shows a cone made from alumina paste and right image shows two cones made from zirconium diboride.

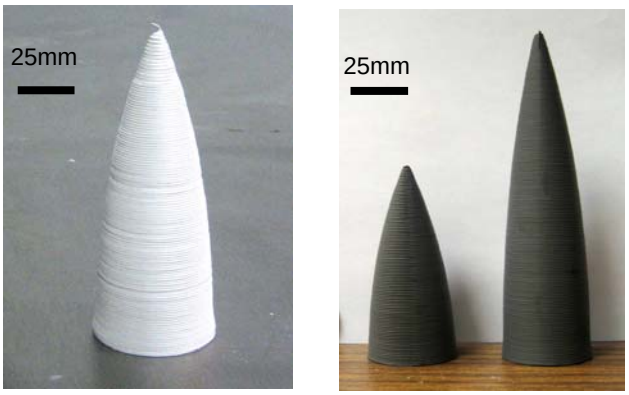

Figure 10: An Al_2O_3 and two ZrB_2 tangent ogive hollow cones in the green state.

4. Summary and Conclusions

The fabrication temperature has been found to significantly affect the material extrusion and deformation behavior in the aqueous based extrusion fabrication process. Fabricating samples at -20 °*C* allows the deposited paste to freeze. This results in the lowest minimum deposition angle, which means the highest self-sustaining ability (without the use of support material). The minimum deposition angle is mainly decided by the environment temperature. The lower the environmental temperature is, the smaller the minimum deposition angle will be. This means the FEF process can fabricate larger parts at -20 °C than at 0 °*C*. By using the heater to prevent paste from freezing, the model time constants and gains are both smaller than the model time constants and gains at 0 °*C*. Therefore at -20 °*C*, with the use of a paste heater, the paste is easier to extrude. Further, the system response is faster than at 0 °*C* without the paste heater. Figure 10 shows two ogive cones in green state fabricated at -20 °*C*. Successful tangent ogive cone fabrications from alumina and zirconium diboride pastes, demonstrated the feasibility of the FEF process at -20 °*C*.

5. Acknowledgement

This work was supported by the Air Force Research Laboratory under Contract FA8650-04-C-5704.

6. References

1. T. S. Huang, “Fabrication of Ceramic Components Using Freeze-form Extrusion Fabrication,” *Ph.D. Dissertation*, Department of Materials Science and Engineering, University of Missouri-Rolla, (2007).

2. G. M. Lous, I. A. Cornejo, T. F. McNulty, A. Safari, and S. C. Danforth, “Fabrication of Piezoelectric Ceramic/Polymer Composite Transducers Using Fused Deposition of Ceramics,” *J. Am. Ceram. Soc.,* 83 [1] 124-28 (2000).

3. J. J. McIntosh, S. C. Danforth and V. R. Jamalabad, “Shrinkage and Deformation in Parts Manufactured by Fused Deposition of Ceramics, “*Proceedings of the Solid Freeform Fabrication Symposium*, The University of Texas at Austin, Austin, TX, August 11-13, 159-166 (1997).

4. T. Himmer, T. Nakagawa and H. Noguchi, “Stereolithography of Ceramics,” *Proceedings of the Solid Freeform Fabrication Symposium*, The University of Texas at Austin, Austin, TX, August 11-13, 363-369 (1997).

5. E. M. Sachs, M. J. Cima, J. Bredt, and A. Curodeau, “CAD-Casting: The Direct Fabricaion of Ceramic Shells and Cores by Three Dimensional Printing,” *Man. Rev.,* 5 [2] 117-126(1992).

6. J. Grau, J. Moon, S. Uhland, M. Cima and E. Sachs, “High Green Density Ceramic Parts Fabricated by the Slurry-Based 3DP Process,” *Proceedings of the Solid Freeform Fabrication Symposium*, The University of Texas at Austin, Austin, TX, August 11-13, 371-378 (1997).

7. J. P. Kruth, P. Mercelis, L. Froyen, and M. Rombouts, “Binding Mechanisms in Selective Laser Sintering and Selective Laser Melting” *Rapid Prototyping J.*, 11[1]26-36 (2005).

8. P. K. Subramanian, J. W. Barlow and H.L. Marcus, “Effect of Particle Size on SLS and Post-Processing of Alumina with Polymer Binders,” *Proceedings of the Solid Freeform Fabrication Symposium*, The University of Texas at Austin, Austin, TX, August 7-9,346-352 (1995).

9. T. S. Huang, M. S. Mason, G. E. Hilmas, and M. C. Leu, “Freeze-form Extrusion Fabrication of Ceramics,” *Virtual and Physical Prototyping*, 1 [2], 93-100 (2006).

10. G. Sui, “Modeling and Analysis of Rapid Freeze Prototyping,” *PhD Dissertation*, University of Missouri-Rolla, Rolla, Missouri (2002).

11. F. Bryant, G. Sui, and M. C. Leu, “A Study on the Effects of Process Parameters in Rapid Freeze Prototyping,” *Proceedings of Solid Freeform Fabrication Symposium*, August 5-7, Austin, Texas, 635-642 (2002).

12. M. C. Leu, W. Zhang, and G. Sui, “An Experimental and Analytical Study of Ice Part Fabrication with Rapid Freeze Prototyping,” *Annals of the CIRP*, 49 [1], 147-150 (2000).

13. G. Sui, and M. C. Leu, “Investigation of Layer Thickness and Surface Roughness in Rapid Freeze Prototyping,” *ASME Journal of Manufacturing Science Engineering*, 125 [3], 555-563 (2002).

PAPER II

Adaptive Control of Freeze–form Extrusion Fabrication Process

Xiyue Zhao, Robert G. Landers and Ming C. Leu

Department of Mechanical and Aerospace Engineering

University of Missouri–Rolla, Rolla, Missouri, 65401–0050

{xzd2c;landersr;mleu}@umr.edu

Abstract

Freeze–form Extrusion Fabrication (FEF) is an additive manufacturing process that extrudes high solids loading aqueous ceramic pastes in a layer–by–layer fashion below the paste freezing temperature for component fabrication. Due to effects such as the air bubble release, agglomerate breakdown, change in paste properties during extrusion as a result of liquid phase migration, etc., the extrusion force is difficult to control. In this paper, an adaptive controller is proposed to regulate the extrusion force. Recursive Least Squares is used to estimate extrusion force model parameters during fabrication and a low–order control scheme capable of tracking general reference trajectories is designed and implemented to regulate the extrusion process. The controller is implemented for sinusoidal, triangular, and square reference trajectories over a wide range of frequencies and to fabricate several parts. The results show the excellent tracking performance of the adaptive controller.

Keywords: Ceramic Paste Extrusion, Solid Freeform Fabrication, Adaptive Control

1. Introduction

Solid Freeform Fabrication (SFF) has tremendous potential for becoming an efficient and inexpensive manufacturing technique for 3–D ceramic component fabrication since it is a tool–less fabrication process and, as compared to conventional fabrication techniques, does not require costly and time–consuming mold preparation. Most SFF techniques for ceramic component fabrication involve the use of organic binders. In some processes, such as the Fused Deposition of Ceramics (FDC) process, the binder content may be as high as 40 to 50 vol.%. The organic binder must be removed during post processing. The binder removal is very time–consuming and generates harmful wastes that are undesirable for the environment [1].

Freeze–form Extrusion Fabrication (FEF) uses an aqueous ceramic paste with a solids loading up to 50 vol.%; however, water is the main liquid medium and the organic binder content is only 2–4 vol.% [2]. In FEF, an aqueous–based ceramic paste is extruded using a ram extruder and deposited on a substrate. After the deposition of each layer, the extrusion mechanism moves up one layer thickness and the next layer is deposited. When fabrication is complete, the part is freeze–dried to prevent crack formation during the drying process. After freeze–drying, the binder is then removed in a rapid heating cycle because of the low binder content. Finally, the parts are sintered at a high temperature (e.g., 1550°C for Alumina). Because the organic binder content is reduced to 2–4 vol.%, FEF is an environmentally friendly paste extrusion technique for ceramic part fabrication.

Most research studies in extrusion processes are concerned with screw extrusion of polymer (melt) extrusion processes. In these processes, in–process measurement of viscosity and throughput (extrusion rate) is generally not available; therefore, most

research studies have concentrated on indirect control of these variables via the regulation of melt temperature and pressure. Costin [3] gave a critical review of the early dynamics and control work in this area, which focused on classical control techniques. Hassan and Parnaby [4] used optimization and off–line curve fitting of the experimental data to define a quasi–linear steady–state model. A cascade controller with one–step–ahead forecasts of melt temperature and melt pressure calculated and changed the set points of the screw speed, barrel/die wall temperature, and restrictor valve angular position to maintain the desired extrusion rate. Costin and Taylor [5] used step tests and pseudo–random binary sequence (PRBS) tests to determine the empirical models of melt temperature and pressure in a single screw extruder (SSE). A PI controller was implemented to remove the long–term drift in the pressure level. More recently, Previdi [6] used step tests to determine an empirical first–order model from voltage (screw speed) to pressure and implemented a digital PID controller. The results showed the controller was able to regulate the pressure at a desired constant reference value. These linear techniques generally cannot capture the system's nonlinearities; therefore, they are only suitable for a specific operating point. Some nonlinear modeling techniques such as artificial neural networks, black box Nonlinear Autoregressive Network (NARX) and, more recently, grey box NARX [7] were proposed. However, these techniques are generally highly dependent on the training data and, thus far, no controllers have been designed and implemented using these models.

Screw extrusion cannot be utilized for ceramic processing since ceramic pastes are abrasive and will severely damage the threads, eventually causing the screw extruder to fail. For ram extrusion, the pressure gradation and unstable shear stress regimes are

much more complex. Modeling and controlling the extrusion pressure of the liquid–solid phase paste generally presents more difficulties, as compared to polymer extrusion, because of unpredictable disturbances such as air bubble release and agglomerate breakdown, material property uncertainties generated during the paste preparation procedures, and the complex variation of paste properties during extrusion due to liquid phase migration [8–12]. Post–operative statistical techniques such as standard error of signal, outlier, spectral and fractal analyses have been used to monitor and model the fluctuations in the ram extrusion pressure signals caused by air bubble release, surface cracking, poor mixing, agglomerate breakdown, etc. [13–18]. However, these approaches are still in the development stage and only a few of them have been applied to effectively provide and implement a control strategy due to the previously addressed control difficulties. Detailed initial modeling and control work for this ram extrusion process can be found in previous publication [19,20].

The rest of the paper is organized as follows. First, the experimental system and FEF process are described. Next, variation in the force extrusion model parameters is investigated experimentally. In the fourth section the adaptive extrusion force controller is designed and its performance is analyzed. Several parts are fabricated using the controller in the final section.

2. Experimental System and Process Parameters and Disturbances

The experimental system consists of three subsystems: gantry motion system, extrusion mechanism, and temperature control system. These subsystems and the disturbances that affect the FEF process are described in this section.

2.1. Hardware and Software Systems

The motion system, shown in Figure 1, consists of a gantry with three orthogonal linear axes (Velmex BiSlide), each with a 250 *mm* travel range. The X–axis consists of two parallel slides and is used as the support for the Y–axis. The Z–axis is mounted on the Y–axis and the extrusion mechanism is mounted on the Z–axis. All axes have limit switches on both ends. Four DC motors (Pacific Scientific PMA22B) drive the axes, each with a resolver for position feedback. The signal sent from the resolver is converted by a resolver–to–digital encoder converter. Each motion axis has a maximum speed of 127 *mm*/*s* and a resolution of 2.54 μm. The axes are controlled by a Delta–Tau Turbo PMAC (Programmable Multi–Axis Controller) PCI board. The axis command voltages are sent from 16 bit Digital to Analog Converters (DACs) with ranges of ±5 *V*.

The extrusion mechanism is shown in Figure 1. It is a ram extruder driven by a DC motor (Kollmorgen AKM23D), which has an encoder with a resolution of 0.254 μm. The input signal to the ram axis drive is voltage from a 16 bit DAC with a range of ±5 *V*. The control signal is limited to a range of ±610 *mV* to prevent system damage due to excessive ram speeds. A load cell (Omega LC305–1KA) is mounted between the plunger and the ram extruder to measure the extrusion force. A 16 bit analog–to–digital conversion board (Delta–Tau ACC28) with a voltage range of ±5 *V* converts the analog signal from the load cell into a digital signal in the PMAC board. The force measurement resolution is 2.2 *N*.

The motion gantry system is housed inside a freezer. A condenser maintains the environmental temperature at 0°*C* (± 2°*C*). Liquid nitrogen can be used to lower the environmental temperature below 0°*C* to –30°*C*. A temperature controller (Omega

CN132) is used to control the environmental temperature by turning a solenoid valve on and off, which regulates the flow rate of liquid nitrogen. As shown in Figure 2, heating coils are installed around the material reservoir and the nozzle to keep the paste temperature at approximately 10–15°C to prevent it from freezing and ensure continuous extrusion.

Control of the motion gantry system is realized by embedded Proportional plus Integral plus Derivative (PID) controllers on the PMAC control board. Estimation and control algorithms for the extrusion mechanism are implemented in PLC programs, which are also provided by the PMAC control system, and can be programmed to implement customized algorithms. Since the PMAC control environment is originally designed for motion control, PLC programs have a lower priority than the motion controllers and are typically executed asynchronously. However, timers can be used to ensure a constant sample rate. In the experiments conducted in this paper, the extrusion force control loop is executed at 10 Hz. The control system schematic is shown in Figure 3.

2.2. Process Parameters

The FEF operation process parameters include reference extrusion force, reference extrusion force derivative, deposition path offset distance, standoff distance (i.e., layer thickness), table speed, and environmental temperature. The path offset distance and standoff distance are mainly determined by the nozzle size. Since 580 μm diameter nozzles are used for the experiments conducted in this paper, the path offset distance and standoff distance are both empirically determined to be 500 μm for proper deposition. For proper part fabrication the table speed must be matched to the extrusion

force. For a given extrusion force, if the table speed is too high fully dense tracks will not be formed and, if the table speed is too low, the ceramic bead will be too large and cover the nozzle. The table speed is set to 10 mm/s for the experiments conducted in this paper such that operation productivity is maintain without the need for an excessive extrusion force. Environmental temperature will affect the rheological properties of the extrudate. The environmental temperature is set to $0°C$ for the experiments conducted in this paper. See [21] for further details of the effect environmental temperature has on FEF processes.

Similar to other studies, extrusion force (pressure) is selected to be the controlled variable because it directly affects the extrusion rate. The larger the extrusion force, the higher the extrusion rate, and vice versa. An experiment was performed to explore the extrusion force operating range. A constant voltage of 30 mV is sent to the ram motor amplifier and the result is shown in Figure 4. The extrusion force continuously increases until it reaches 2002 N at 219.1 sec, and then suddenly drops to 1252 N. It was observed that the paste began to come out from the top of the material reservoir due to the large extrusion force. After this occurred, the paste continuously extruded from both the nozzle and the top of the material reservoir and the extrusion force remained at approximately 1160 N. Therefore, the maximum extrusion force should not exceed 2002 N. According to operator experience, the maximum extrusion force is set to 1558 N, which is large enough for normal operation and low enough to protect the extrusion mechanism.

Reference extrusion force derivative is another important process parameter. Typically, the initial reference extrusion force is manually selected to be between 315 and 405 N, depending on paste properties, which vary from batch to batch. The higher the paste apparent viscosity, the larger the initial reference extrusion force. It is necessary to

continually increase the reference extrusion force during the operation to maintain a constant extrusion rate. Experiments show that the extrusion rate slowly decreases as the amount of paste in the material reservoir reduces when the extrusion force is maintained constant. Since the table speed is constant during fabrication, the decrease in extrusion rate may result in under–filling, generating discontinuous paste flow in the building area as shown in Figure 6. Nozzle clogging may even occur. It is believed that the continuous decrease of extrusion rate is related to liquid phase migration during the extrusion process [8]. The extrusion force causes a redistribution of the paste liquid and solid phases during the extrusion process, subsequently changing the paste rheological property (typically the paste apparent viscosity will increase). When the paste is compressed, the water moves toward the die region more quickly than the paste; therefore, the water content becomes highest in the die region and decreases until it is a minimum at the top of the material reservoir. This change will affect the extrusion rate. Typically, the reference extrusion force will need to be increased to maintain the desired extrusion rate [9–12]. The reference extrusion force derivative is selected to be $2.2 \cdot 10^{-2}$ N/s, from operator experience, for the experiments conducted in this paper.

2.3. Process Disturbances

Disturbances affecting the FEF process include liquid phase migration, agglomerate breakdown, and air bubble release. Liquid phase migration causes the paste to become drier during the operation and, thus, become more difficult to extrude, as discussed above. Regardless of how well the paste is prepared, it will always contain agglomerates (i.e., groups of ceramic particles) and air bubbles. When the ram is applied to the paste, the agglomerates will “slide” past one another in the material reservoir,

which will cause the agglomerates to break into smaller agglomerates and cause fluctuations in the extrusion force. Further, based on experimental observations, a large agglomerate breakdown in the nozzle region will cause the extrusion force to increase. As the air bubbles migrate towards the nozzle, they join together and, when an air bubble leaves the nozzle, the extrusion force drops. This affect is shown in Figure 5. In this experiment the periodic voltage signal sent to the ram motor drive was 21.4 *mV* for 10 s*ec*, –9.2 *mV* for 5 s*ec*, 18.3 *mV* for 15 s*ec*, and –6.1 *mV* for 5 *sec*. The extrusion force fluctuated periodically and, when an air bubble release occurred at 1836 *sec*, the extrusion force suddenly dropped from 285 *N* to 55.9 *N*, and then slowly increased to the previous range.

3. Model Parameter Variations in FEF Processes

The FEF process contains many disturbances, as described above. Also, the paste composition is slightly different from batch to batch due to variations in the preparation, which includes material mixing and ball milling, and cannot be totally eliminated. Storage time and environmental conditions, such as temperature and humidity, also affect the paste properties. In this section Recursive Least Squares (RLS) is applied to the FEF extrusion force process to estimate the dynamic model parameters for different batches of paste, and for a single reservoir of paste as it is completely extruded, to analyze variations in the model parameters for different batches and as the amount of paste in the reservoir changes.

Alumina paste is utilized for all of the experiments conducted in the paper. The paste is a combination of Al2O3 powder, PEG, glycerol, Darvan C, and water. The components are mixed and then ball milled for twenty–four hours to break up

agglomerates and produce a uniform mixture. Aquazol is dissolved in water at 60°*C* using magnetic stirring to form a 50 vol.% Aquazol solution. The Aquazol solution is added using a vacuum mixer (Whip Mix, Model F) to minimize bubbles. The final viscosity is adjusted by adding acid to control the paste pH.

3.1. Model Parameter Estimation

It has been shown that the ceramic paste extrusion force dynamics can be characterized as a first–order dynamic system [19]. The digital transfer function of a first–order system is

$$G(z) = \frac{F(z)}{u(z)} = \frac{K(1-a)}{z-a} \tag{1}$$

where z is the forward shift operator, F is the extrusion force (N), u is the command voltage (mV) sent to the ram motor amplifier, K is the model gain (N/mV), which is unknown. The parameter a is also unknown and is related to the time constant. The difference equation corresponding to Eq. (1) is

$$F(k) = aF(k-1) + K[1-a]u(k-1) = \boldsymbol{\eta}(k-1)\boldsymbol{\varphi}(k-1) \tag{2}$$

where k is the iteration number and the unknown parameter and regression variable vectors, respectively, are

$$\boldsymbol{\eta} = \begin{bmatrix} a & K(1-a) \end{bmatrix} = \begin{bmatrix} a & b \end{bmatrix} \tag{3}$$

$$\boldsymbol{\varphi} = \begin{bmatrix} F(k-1) & u(k-1) \end{bmatrix}^T \tag{4}$$

Parameter estimates are then computed recursively using the following equations

$$\mathbf{q}(k) = \mathbf{P}(k-1)\boldsymbol{\varphi}(k)\left[\mathbf{I} + \boldsymbol{\varphi}^T(k)\mathbf{P}(k-1)\boldsymbol{\varphi}(k)\right]^{-1} \tag{5}$$

$$\hat{\boldsymbol{\eta}}(k) = \hat{\boldsymbol{\eta}}(k-1) + \mathbf{q}(k)\left[y(k) - \boldsymbol{\varphi}^T(k)\hat{\boldsymbol{\eta}}(k-1)\right] \tag{6}$$

$$\mathbf{P}(k) = \left[\mathbf{I} - \mathbf{q}(k)\boldsymbol{\varphi}^T(k)\right]\mathbf{P}(k-1) \tag{7}$$

where $\hat{\boldsymbol{\eta}}(k)$ is the estimated parameter vector. The matrix **I** is a two–by–two identity matrix. The matrix **P** is known as the covariance matrix. The initial covariance matrix is typically selected to be a large positive definite diagonal matrix. In the experimental studies conducted in this paper, $\mathbf{P}(0) = \begin{bmatrix} 1000 & 0 \\ 0 & 1000 \end{bmatrix}$ and covariance resetting is not applied. In this form, RLS can be applied to experimental data to estimate the model parameters *a* and *b*. The time constant and gain, respectively, are derived from the estimated model parameters as

$$\tau = -\frac{T}{\ln(a)} \tag{8}$$

$$K = \frac{b}{1-a} \tag{9}$$

where *T* is the sample period.

An experiment is conducted to investigate the ability of RLS to estimate FEF extrusion force process model parameters. The input voltage to the ram motor amplifier is 18.3 *mV* for 15 *sec*, –6.1 *mV* for 5 *sec,* 21.4 *mV* for 10 *sec*, and –9.2 *mV* for 5 *sec*. Positive and negative input voltages donate advancing and retreating ram motions, respectively. Note that the magnitudes of the positive and negative inputs are not equal. Since it typically requires more energy for the ram to advance than to retreat, the magnitude in the positive direction is greater than the magnitude in the negative direction in an attempt to maintain a constant average extrusion force. By using Eqs. (5)–(7), the model parameters are estimated and the modeled output is computed and compared with

the measured output, as shown in Figure 7. It can be seen that the modeled extrusion force matches the real extrusion force well.

3.2. Model Variation Analysis

As previously mentioned, paste compositions are slightly different from batch to batch. A similar phenomenon was also reported by Costin [5]. To investigate the effect paste batch preparation has on the force extrusion model parameters, model parameters for four reservoirs of paste, each from a different batch, are estimated. Each experiment starts with a reservoir of unused paste with an initial volume of approximately 40 *ml*. The command voltage to the ram motor amplifier periodically changes between constant values of –3.7 and 8.5 *mV* every 5 *sec*. The time constants and gains are calculated using Eqs. (5)–(9). Each experiment is conducted for 120 *sec* and the average time constants and gains are shown in Table 1. It can be seen that both model parameters are very different for the four batches of paste.

Even for the same batch of paste, the paste properties for different reservoirs of paste will be different because of the variations in storage time, temperature, humidity, etc. Moreover, for the same tube of paste, the paste properties will also change during the extrusion process, as reported in [8]. Experiments are conducted to investigate how the extrusion dynamic model parameters vary during the FEF process as the amount of paste in the material reservoir decreases. In these experiments, a reservoir of paste with an initial volume of approximately 35 *ml* is extruded. The command voltage changes periodically and is 12.2 *mV* for 10 *sec*, –6.1 *mV* for 5 *sec*, 6.1 *mV* for 10 *sec*, and 0 *mV* for 5 *sec* for each experiment, and approximately 5 *ml* of paste is extruded over a period of

approximately 2000 *sec*. Average time constants and gains (shown in Table 2) were calculated from the last 100 *sec* of data collected for each experiment.

Figure 8 shows that as the volume of paste in the material reservoir decreases the time constant decreases and the gain increases. It is hypothesized that the changes in the time constant and gain as paste is extruded are associated with changes in the paste rheological properties. As paste is extruded, liquid phase migration causes the paste to become drier and air bubble release causes the paste to become stiffer. These effects will cause the paste to become less elastic and more viscous; therefore, the time constant decreases and less time is required for the extrusion force to reach the steady–state. Also, as the paste becomes less elastic and more viscous, it is harder to compress, and the gain will increase.

These experiments demonstrate that different batches of paste have much different extrusion force dynamic properties and that even for the same reservoir of paste, the extrusion force dynamic properties change substantially as the amount of material in the reservoir decreases. Therefore, an adaptive control scheme is adopted in this paper to account for the inherent model parameter variations by updating the controller gain calculated from the model parameters in real time. Also, the smallest time constant for the force extrusion process is approximately 61.4 seconds, as shown in Table 2. Therefore, a sample rate of 10 *Hz* is more than sufficient for this process.

4. Adaptive Force Extrusion Controller

An adaptive general tracking controller that will be used to regulate the extrusion force for FEF processes is designed and discussed in this section.

4.1. Tracking Controller Design

The extrusion force model is

$$F(k) = aF(k-1) + bu(k-1) \tag{10}$$

The error is

$$e(k) = F_r(k) - F(k) \tag{11}$$

where F_r is the reference extrusion force. Substituting Eq. (11) into Eq. (10)

$$e(k) = F_r(k) - aF(k-1) - bu(k-1) \tag{12}$$

Noting that $e(k–1) = F_r(k–1) – F(k–1)$, solving for $F(k–1)$ and substituting this expression into Eq. (12)

$$e(k) = ae(k-1) + F_r(k) - aF_r(k-1) - bu(k-1) \tag{13}$$

Defining the pseudo control signal $\mu(k–1) = F_r(k) – aF_r(k–1) – bu(k–1)$, Eq. (13) can be rewritten as

$$e(k) = ae(k-1) + \mu(k-1) \tag{14}$$

A controller of the form $\mu(k–1) = ge(k–1)$ is used where the controller gain g is adjusted to shape the closed–loop transient response. In the adaptive control scheme, the model parameters a and b are estimated in real time and the controller gain g is updated in real time given the estimated value of a

$$g = \exp\left(-\frac{T}{\tau_d}\right) - \hat{a} \tag{15}$$

where τ_d is the desired closed–loop time constant. The physical control signal is

$$u(k-1) = \frac{F_r(k) - \hat{a}F_r(k-1) - ge(k-1)}{\hat{b}} \tag{16}$$

Note that this controller requires future knowledge of the reference signal, which is typically available. The controller is able to intelligently modify its gain to maintain stability and a consistent transient response as the extrusion force process varies. Also, when different batches of paste and reservoirs of material are used, the adaptive controller can quickly estimate the model parameters and adjust its gain.

4.2. General Tracking Controller Performance

The general tracking controller is implemented in PLC programs of the Turbo PMAC control system. The control law is proved (see Appendix) to be able to achieve a unitary closed–loop transfer function, assuming zero initial conditions. Therefore, theoretically, this controller extends the tracking bandwidth to infinity. Practically, the system tracking bandwidth is limited due to unmodeled dynamics, control signal magnitude limitation, disturbances, etc. To investigate controller performance, experiments with three different reference signals (i.e., sinusoidal, triangular, and square) are conducted. The closed loop time constant is selected to be 0.1 *sec*, to achieve the fastest response possible given the sampling limitations. All experiments were conducted using the same batch of alumina paste.

4.2.1. Sinusoidal Reference

Sinusoidal reference extrusion forces with frequencies ranging from 0.1 to 1 *Hz* and peak–to–peak amplitudes of 89 *N* are utilized in the first set of experiments. Figure 9 shows the extrusion force and control signal responses for a reference with a frequency of 0.1 *Hz*. It can be seen that there are some fluctuations in the control signal ranging from –250 to 200 *mV*. The fluctuations of the control signals coincide with the fluctuations of the measured force feedback. Figure 10 shows the extrusion force and control signal

responses for a reference with a frequency of 1 *Hz*. The controller sample rate is 10 *Hz,* so there are 10 samples/cycle for the reference with a frequency of 1 *Hz*, much less than the 100 samples/cycle for the reference with a frequency of 0.1 *Hz*. Therefore, the fluctuations in the measured force signals are significantly reduced and, subsequently, the fluctuations in the control signals are much less. Since more control energy is required to track the reference with the higher frequency, the control signal is larger and is between –500 to 500 *mV*.

The data is used to create magnitude and phase frequency plots of the closed–loop system, as shown in Figure 11. The magnitude is between –0.05 and 0.21 *dB* and tends to decrease as the frequency increases. The phase is zero for low frequencies, decreases slightly as the frequency increases, and is –9.8° for a frequency of 1 *Hz*. Figure 12 shows the extrusion force average error and standard deviation of the average error. The average error is between 0.053 and –0.115 *N* and is not correlated with frequency. The standard deviation increases as the frequency increases and varies from 1.31 *N* for a frequency of 0.1 *Hz* to 4.73 *N* for a frequency of 1.0 *Hz*.

4.2.2. Triangular Reference

Triangular extrusion force references with frequencies ranging from 0.1 to 1 *Hz* and peak–to–peak amplitudes of 89 *N* are utilized in these experiments. Figure 13 shows the extrusion force and control signal responses for a reference with a frequency of 0.1 *Hz*. The control signals range from –130 to 150 *mV*. Figure 14 shows the extrusion force response for the reference with a frequency of 1 *Hz*. As more control energy is used to perform the higher frequency tracking, the control signals are between –250 to 200 mV, larger than those in Figure 13.

The data is used to create magnitude and phase frequency plots of the closed–loop system, as shown in Figure 11. The magnitude is between –0.301 and 0.051 *dB* and tends to decrease as the frequency increases. The phase is zero for low frequencies, decreases slightly as the frequency increases, and is –11.9° for a frequency of 1 *Hz*. Figure 12 shows the extrusion force average error and standard deviation of the average error. The average error is between –0.018 and 0.078 *N* and is not correlated with frequency. The standard deviation increases as the frequency increases and varies from 1.19 *N* for a frequency of 0.1 *Hz* to 3.74 *N* for a frequency of 1.0 *Hz*.

4.2.3. Square Reference

Square reference extrusion forces with frequencies ranging from 0.1 to 1 *Hz* and peak–to–peak amplitudes of 89 *N* are utilized in this set of experiments. Figure 15 shows the extrusion force and control signal responses for a reference with a frequency of 0.1 *Hz*. It can be seen that the control signal saturates at –610 and 610 *mV* for approximately 0.09 *sec* when the reference signal decreases and increases, respectively. However, the steady–state control signal is between –30 and 30 *mV*. The rise time is approximately 0.14 *sec*. Figure 16 shows the extrusion force and control signal responses for a reference with a frequency of 1 *Hz.* As the reference changes values, the control signal saturates between –610 to 610 *mV* for about 0.09 *sec*, similar to Figure 15. The rise time is 0.102 *sec*, similar to that for that of the reference with the frequency of 0.1 *Hz*, due to the control signal saturation.

The data is used to create magnitude and phase frequency plots of the closed–loop system, as shown in Figure 11. The magnitude is between –0.115 and 0.204 *dB* and tends to decrease as the frequency increases. The phase is -0.15^0 for low frequencies, decreases

slightly as the frequency increases, and is –15.1° for a frequency of 1 *Hz*. Figure 12 shows the extrusion force average error and standard deviation of the average error. The average error is between –0.094 and 0.137 *N* and is not correlated with frequency. The standard deviation increases as the frequency increases and varies from 2.81 *N* for a frequency of 0.1 *Hz* to 8.06 *N* for a frequency of 1.0 *Hz*. The larger phase shifts and error standard deviations, as compared to the experiments with sinusoidal and triangular references, are due to the fact that saturation occurred whenever the reference extrusion force changed values.

4.2.4. Discussion

At steady–state, the control signal is very small, usually between –50 to 50 *mV* according to the experimental results. Therefore, the controller only utilizes a very small range of the operation range of the ram motor control signal, which is –5 to 5 *V*. Therefore, the ram motor rotates at a very low speed, and motor commutation will cause fluctuations in the ram velocity, which will directly affect the extrusion force.

5. Summary and Conclusions

Recursive Least Squares (RLS) was applied to estimate the parameters of a first–order dynamic model of the Freeze–form Extrusion Fabrication process in real time. An adaptive controller with a general tracking control law was designed and implemented to regulate the extrusion force. Experiments with sinusoidal, triangular, and square extrusion force references with different frequencies ranging from 0.1 to 1 *Hz* were conducted to investigate the controller's performance.

The experimental results show the model parameters are not only different from batch to batch, but also change significantly during the extrusion process. It is observed

that the time constant decreases and gain increases as the paste in the material reservoir decreases. The reason for these trends is believed to be related to liquid phase migration. The adaptive controller demonstrated excellent tracking for all reference trajectories over a wide range of frequencies. The adaptive controller provides an automated means to determine the controller parameter when a new batch of paste is utilized and can adjust the controller parameter automatically during the extrusion process to account for disturbances and inherent changes in the process due to liquid phase migration. Estimating the model parameters during the extrusion process also provides a potential technique to monitor the paste property in real time.

6. Acknowledgements

The authors wish to acknowledge the financial support for this work from the UMR Center for Aerospace Manufacturing Technologies (Air Force Research Laboratory contract FA8650–04–C–5704) and the technical support of colleagues at UMR, the Boeing Company, and the Air Force Research Laboratory.

7. References

1. Lous, G.M., Cornejo, I.A., McNulty, T.F., Safari, A., and Danforth, S.C., 2000, “Fabrication of Piezoelectric Ceramic/Polymer Composite Transducers using Fused Deposition of Ceramics,” *Journal of the American Ceramic Society,* **83**(1), pp. 124–128.

2. Huang, T.S., 2007, “Fabrication of Ceramic Components Using Freeze–form Extrusion Fabrication,” Ph.D. Dissertation, Department of Materials Science and Engineering, University of Missouri–Rolla, Rolla, Missouri.

3. Costin, M.H., Taylor, P.A., and Wright, J.D., 1982, “A Critical Review of Dynamic Modeling and Control of Plasticating Extruders,” *Polymer Engineering and Science*, **22**(7), pp. 393–401.
4. Hassan, G.A. and Parnaby, J., 1981, “Model Reference Optimal Steady–State Adaptive Computer Control of Plastics Extrusion Processes,” *Polymer Engineering and Science*, **21**(5), pp. 276–284.
5. Costin, M.H. and Taylor, P.A., 1982, “On the Dynamics and Control of a Plasticating Extruder,” *Polymer Engineering and Science*, **22**(17), pp. 1095–1106.
6. Previdi, F., Savaresi, S.M., and Panarotto, A., 2006, “Design of a Feedback Control System for Real–Time Control of Flow in a Single–Screw Extruder,” *Control Engineering Practice*, **14**(9), pp. 1111–1121.
7. McAfee, M. and Thompson, S., 2007, “A Novel Approach to Dynamic Modeling of Polymer Extrusion for Improved Process Control,” *Proceedings of the Institution of Mechanical Engineers, Part I: Journal of Systems and Control Engineering*, **221**(4), pp. 617–628.
8. Burbidge, A.S., Bridgewater, J., and Saracevic, Z., 1995, “Liquid Migration in Paste Extrusion,” *Chemical Engineering Research and Design*, **73**(7), pp. 810–816.
9. Amarasinghe, A.D.U.S. and Wilson, D.I., 1998, “Interpretation of Paste Extrusion Data,” *Chemical Engineering Research and Design*, **76**(A1), pp. 3–8.
10. Kaya, A. and Rice, L.S., 1982, “Measurement and Control Problems for Extrusion Processes,” *American Control Conference*, Arlington, Virginia, June, 14–16, pp. 1149–1154.

11. Amarasinghe, A.D.U.S. and Wilson, D.I., 1999, “On–Line Monitoring of Ceramic Paste Extrusion,” *Journal of the American Ceramic Society*, **82**(9), pp. 2305–2312.

12. Russell, B.D., Wilson, D.I., Lasenby, J., and Blackburn, S., 2002, “On–Line Monitoring of Pastes Undergoing Extrusion,” *Proceedings of the 4th World Congress on Particle Technology*, Sydney, Australia, July 21–25.

13. Russell, B.D., Lasenby, J., Blackburn, S., and Wilson, D.I., 2004, “Monitoring Structural Aspects of Pastes Undergoing Continuous Extrusion using Signal Processing of Pressure Data,” *Chemical Engineering Research Design*, **82**(6), pp. 770–783.

14. Russell, B.D., Ovaici, H., Lasenby, J., Beckett, S.T., and Wilson, D.I., 2006, “Real–Time Monitoring of Chocolate Extrusion by Signal Processing of Pressure Transducer Data,” *Food Control*, **17**(11), pp. 862–867.

15. Tomer, G. and Newton, J.M., 1999, “Water Movement Evaluation during Extrusion of Wet Powder Masses by Collecting Extrudate Fractions,” *International Journal of Pharmaceutics*, **182**(1), pp. 71–77.

16. Benbow, J.J., Blackburn, S., and Mills, H., 1998, “The Effects of Liquid–Phase Rheology on the Extrusion Behavior of Paste,” *Journal of Materials Science*, **33**(24), pp. 5827–5833.

17. Sherwood, J.D., 2002, “Liquid–Solid Relative Motion during Squeeze Flow of Pastes,” *Journal of Non–Newtonian Fluid Mechanics*, **104**(1), pp. 1–32.

18. Rough, S.L., Wilson, D.I., and Bridgewater, J., 2002, "A Model Describing Liquid Phase Migration within an Extruding Microcrystalline Cellulose Paste," *Chemical Engineering Research and Design*, **80**(A7), pp. 701–714.

19. Mason, M.S., Huang, T.S., Landers, R.G., Leu, M.C., and Hilmas, G.E., 2006, "Freeform Extrusion of High Solids Loading Ceramic Slurries, Part I: Extrusion Process Modeling," *Seventeenth Annual Solid Freeform Fabrication Symposium*, Austin, Texas, August 14–16.

20. Mason, M.S., Huang, T.S., Landers, R.G., Leu, M.C., and Hilmas, G.E., 2006, "Freeform Extrusion of High Solids Loading Ceramic Slurries, Part II: Extrusion Process Control," *Seventeenth Annual Solid Freeform Fabrication Symposium*, Austin, Texas, August 14–16.

21. Zhao, X.Y., Mason, M.S., Huang, T.S., Leu, M.C., Landers, R.G., Hilmas, G.E., Easley, S.J. and Hayes, M.W., 2007, "Experimental Investigation of Effect of Environment Temperature on Freeze–form Extrusion Fabrication," *Eighteenth Annual Solid Freeform Fabrication Symposium*, Austin, Texas, August 6–8.

Table 1: Estimated model time constants and gains for different batches of paste.

Batch	Time constant (*sec*)	Gain (*N*/*mV*)
1	108	761
2	184	410
3	125	825
4	164	550

Table 2: Model time constants and gains for various amounts of paste in material reservoir.

Test	Volume of remaining paste (*ml*)	Time constant (*sec*)	Gain (*N*/*mV*)
1	35	117	794
2	30	110	881
3	25	103	920
4	20	91.2	935
5	15	87.6	980
6	10	61.4	1035

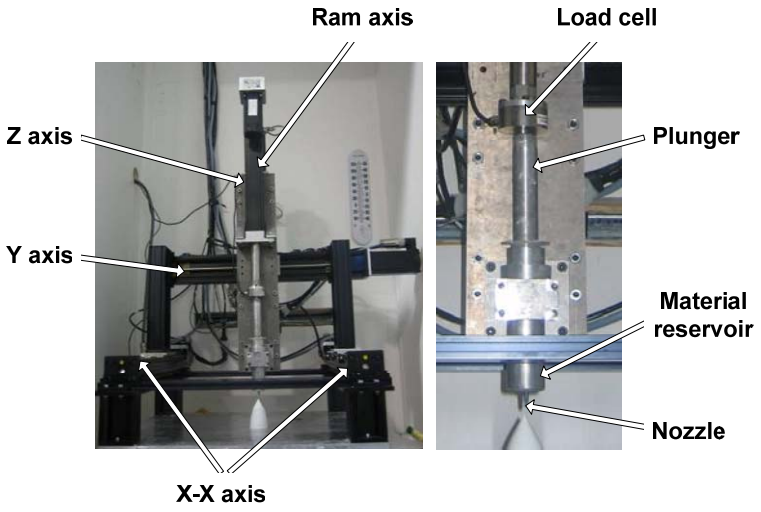

Figure 1: **Gantry motion system (left) and extrusion mechanism (right).**

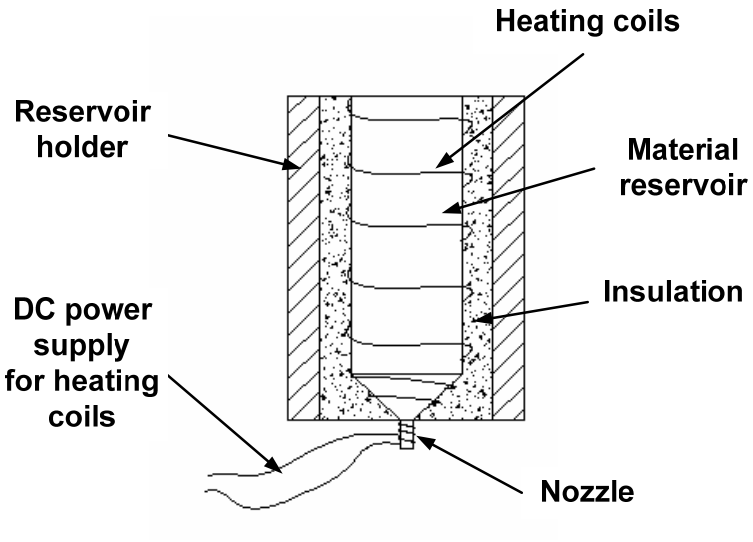

Figure 2: Extrusion mechanism schematic.

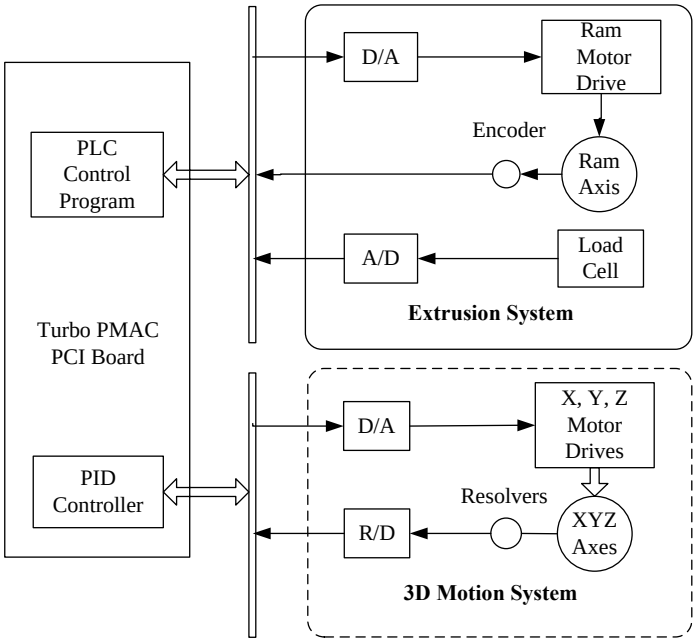

Figure 3: FEF process control system schematic.

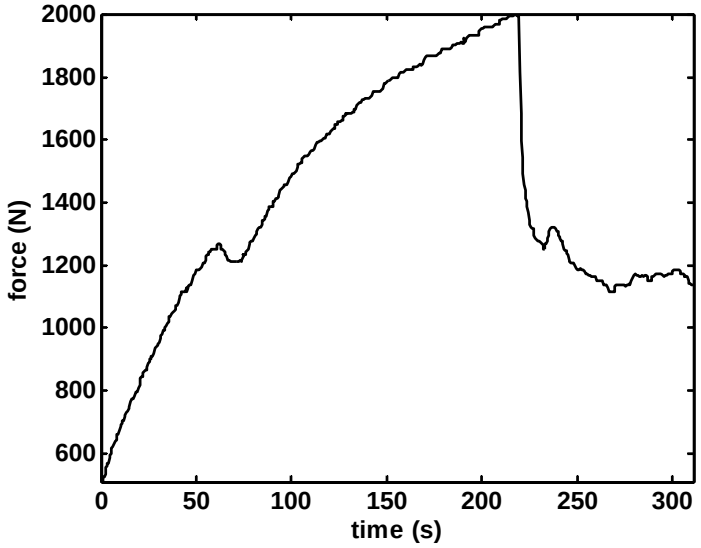

Figure 4: Extrusion force response to a constant command voltage of 30 *mV*.

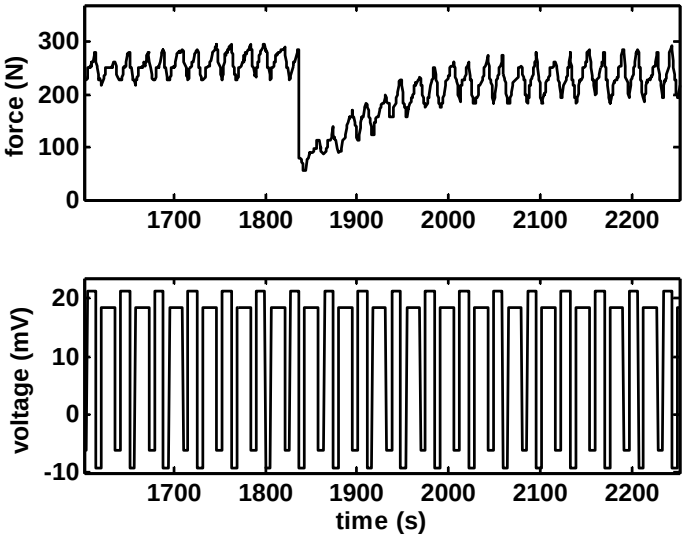

Figure 5: Extrusion force (top) and command voltage (bottom). Sudden drop in extrusion force is due to an air bubble release.

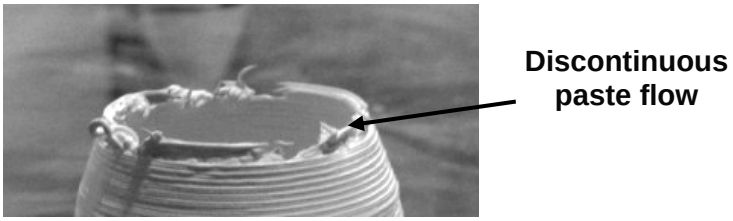

Figure 6: Discontinuous paste flow on top of a hollow cone.

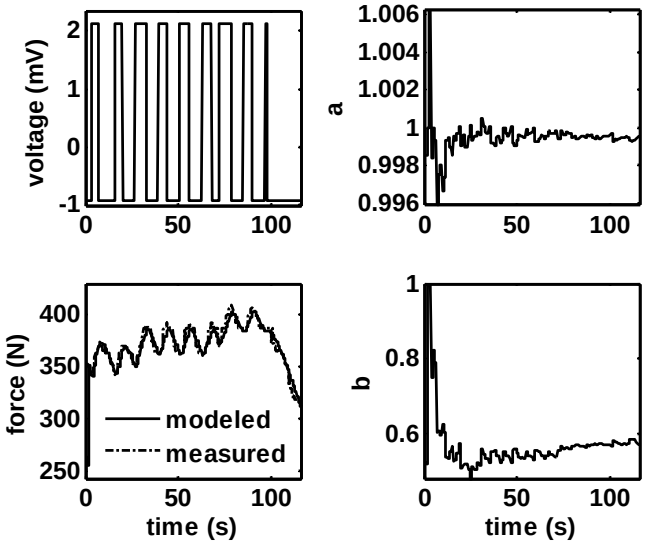

Figure 7: Commanded voltage (upper left), modeled and measured extrusion forces (bottom left), and estimated model parameters *a* (upper right) and *b* (lower right).

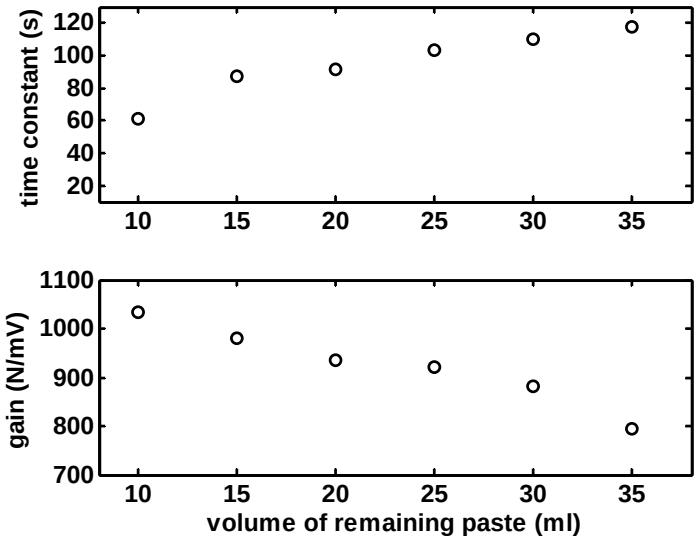

Figure 8: Model time constant (top) and model gain (bottom) as functions of paste volume in material reservoir.

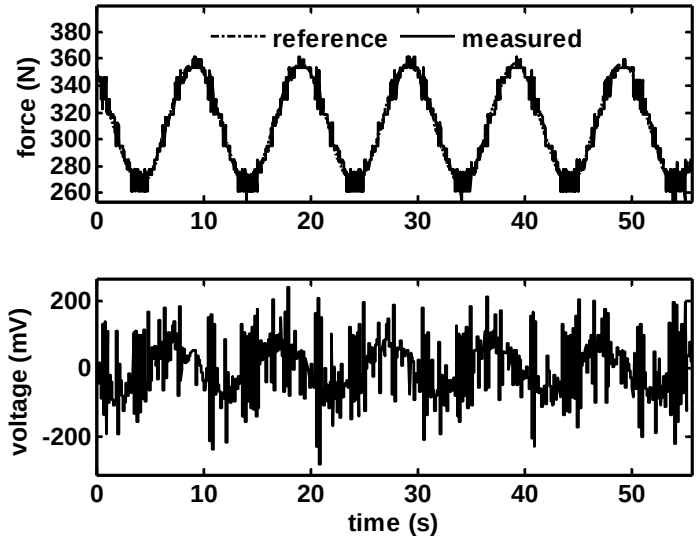

Figure 9: Extrusion force (top) and command voltage (bottom) responses for a sinusoidal reference with a frequency of 0.1 *Hz*.

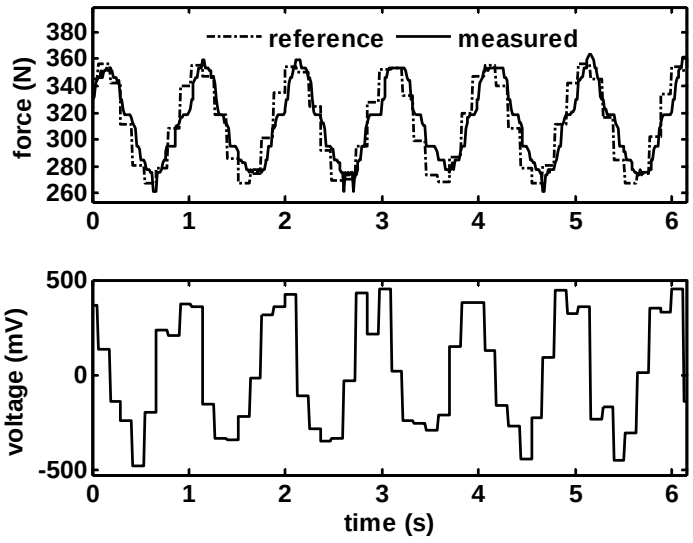

Figure 10: Extrusion force (top) and command voltage (bottom) responses for a sinusoidal reference with a frequency of 1 *Hz*.

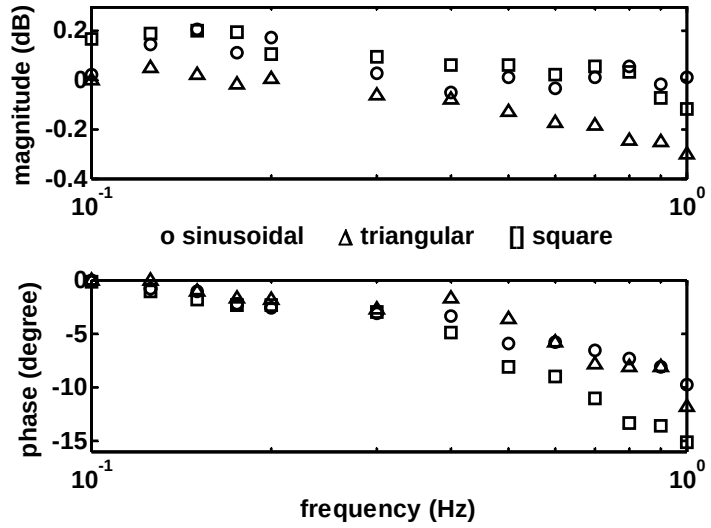

Figure 11: Experimental extrusion force closed–loop magnitude (top) and phase shift (bottom) for sinusoidal, triangular, and square reference extrusion forces.

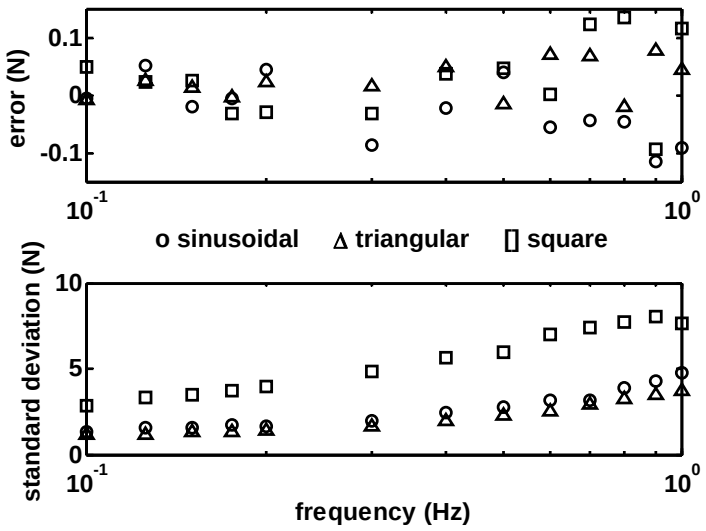

Figure 12: Extrusion force average error (top) and error standard deviation (bottom) for sinusoidal, triangular, and square reference extrusion forces.

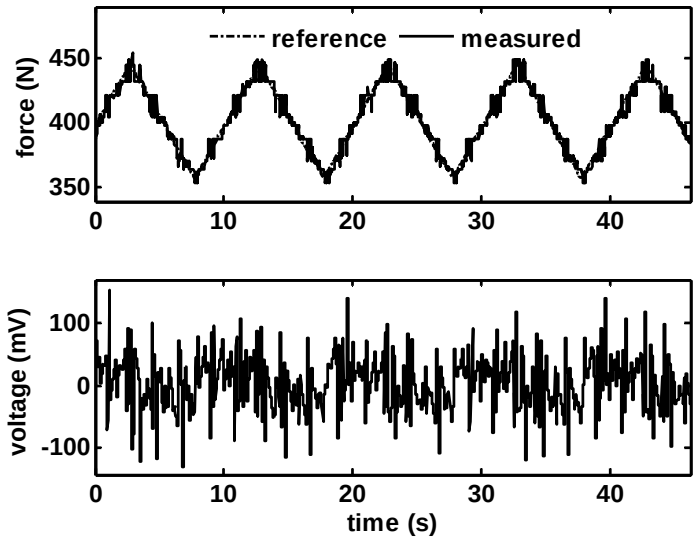

Figure 13: Extrusion force (top) and command voltage (bottom) responses for a triangular reference with a frequency of 0.1 *Hz*.

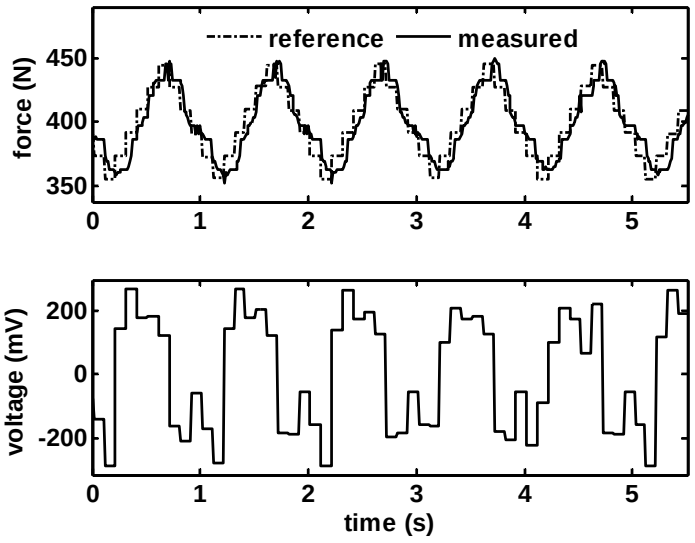

Figure 14: Extrusion force (top) and command voltage (bottom) responses for a triangular reference with a frequency of 1 *Hz*.

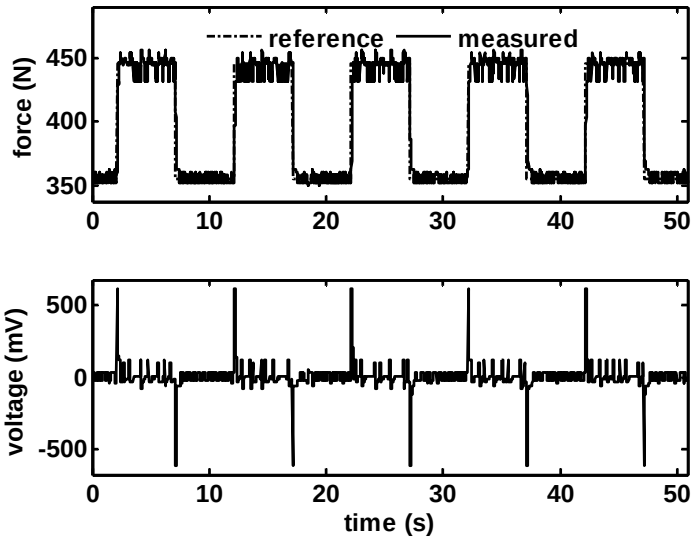

Figure 15: Extrusion force (top) and command voltage (bottom) responses for a square reference with a frequency of 0.1 *Hz*.

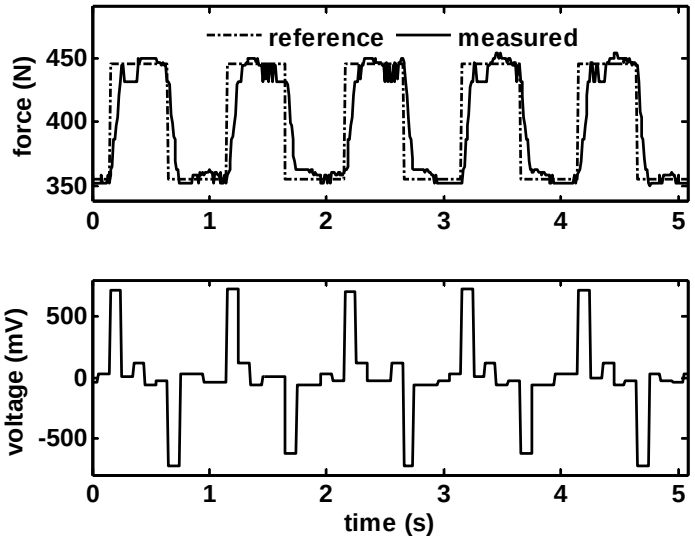

Figure 16: Extrusion force (top) and command voltage (bottom) responses for a square reference with a frequency of 1 *Hz*.

Appendix

The proposed controller's ability to achieve a unitary transfer function is proved in this appendix. Taking the *z*–transform of Eq. (16), assuming no model parameter estimation error

$$bu(z) = F_r(z)z - aF_r(z) - ge(z) \tag{A1}$$

Taking the *z*–transform of the error given in Eq. (11)

$$e(z) = F_r(z) - F(z) \tag{A2}$$

Substituting Eq. (A2) into Eq. (A1) and rearranging

$$bu(z) = [z - a - g]F_r(z) + gF(z) \tag{A3}$$

Taking the *z*–transform of Eq. (10)

$$F(z) = aF(z)z^{-1} + bu(z)z^{-1} \tag{A4}$$

Substituting Eq. (A3) into Eq. (A4) and rearranging

$$\left[1 - az^{-1} - gz^{-1}\right]F(z) = \left[1 - az^{-1} - gz^{-1}\right]F_r(z) \tag{A5}$$

Therefore, the closed–loop transfer function is

$$\frac{F(z)}{F_r(z)} = \frac{1 - az^{-1} - gz^{-1}}{1 - az^{-1} - gz^{-1}} = 1 \tag{A6}$$

VITA

Xiyue Zhao was born on September 18, 1980 in Hei Longjiang, P. R. China. In July 2002, she received her Bacherlor of Science degree in Mechanical and Automation Engineering from University of Aeronautics and Astronautics, Beijing, P. R. China.

Upon completion of her undergraduate degree, she worked at the Beijing Can-Fareast Science & Development Company as project engineer from July 2002 to December 2002 and then worked as mechanical engineer from December 2002 to May 2005.

In August 2005, she began her study for Master's degree in Mechanical and Aerospace Engineering. Her research areas include manufacturing, dynamics and control, rapid prototyping, solid freeform fabrication, and ceramic processing. She received her Master of Science in Mechanical Engineering in University of Missouri-Rolla in December 2007.

After her graduation, she will continuously dedicate herself in the field of mechanical engineering.